Aalto University
School of Chemical
Technology

School of Chemical Technology
Degree Programme of Chemical Technology

Paolo Ponzo

MASS TRANSFER IN THREE-PHASE REACTIVE CRYSTALLIZATION

Final project (30 cr) for the degree of Master of Science in Chemical Technology submitted for inspection, Espoo, 19 May 2015.

Supervisor **Professor Ville Alopaeus**

Instructors **M.Sc. Wenli Zhao**

D.Sc. Kaj Jakobsson

Author Paolo Ponzo

Title of thesis
Mass transfer in three-phase reactive crystallization

Department Biotechnology and Chemical Technology

Professorship Chemical Engineering **Code of professorship** KE-42

Thesis supervisor Ville Alopaeus

Thesis advisor(s) / Thesis examiner(s) Kaj Jakobsson, Wenli Zhao

Date 19.05.2015 **Number of pages** 84 **Language** English

Abstract

Three-phase reactive crystallization is a multi-step process which involves particles dissolution, gas absorption and precipitation.

The purpose of this work is development and comparison of two kind of models for three-phase reactive crystallization. In order to do this, different models for gas absorption and precipitation were coupled with a only dissolution model. The models were compared by their implementation on MATLAB and simulating several experimental conditions from the literature in which $CaCO_3$ and $MgCO_3$ precipitation was operated in $Ca(OH)_2 - H_2O - CO_2$ and $Mg(OH)_2 - H_2O - CO_2$ systems respectively.

In the first simplified model the reactions and precipitation in the film surrounding the gas-liquid interface were assumed to be negligible while in the second kind of model the phenomena occurring in the film were taken into account.

The results obtained showed that the significance of the reactions and precipitation in the liquid film depends on some operational conditions such as the mass transfer resistance and the molar fraction of CO_2 in the gas fed into the system.

In particular in operational conditions in which a high mass transfer resistance is combined with a low concentration of CO_2 in the inlet gas, the reaction and precipitation phenomena were predicted to occur mainly in the film. In this case the use of the simplified model significantly under-estimated of the mass transfer rate.

Keywords
Crystallization, Mass Transfer, Precipitation, Absorption

Aknowledgments

First of all I would like expressing my deepest gratitude to my supervisor Professor Ville Alopaeus for accepting me to work in this department, giving me the opportunity to write my thesis in this great University and for always being available for help and advices.

A special acknowledgment goes also to my instructors Wenli for sharing with me all his knowledge and huge amount of work and Kaj Jakobsson who wisely guided me throughout this project answering all my questions and supporting me constantly.

A giant thanks to all the friends I met here in Finland. Each of them played an essential role in making this period far from home amazing and unforgettable.

Finally the biggest thanks goes to my parents and my super siblings. Because never before this long time far from you I realized how important for me you are.

CONTENTS

List of symbols

a_L	Specific gas-liquid surface area
a_S	Specific solid-liquid surface area
B	Nucleation rate
C_i	Molar concentration of component i
D_i	Diffusivity coefficient of component i
G	Crystals' linear growth rate
g	Exponent of growth rate
k_{i1}	Kinetic constant for the direct reaction r_i
k_{i2}	Kinetic constant for the reverse reaction r_i
K_{SPi}	Solubility product of component i
k_L	Gas-liquid mass transfer coefficient
k_S	Solid-liquid mass transfer coefficient
k_g	Growth rate constant
k_n	Nucleation rate constant
L_0	Size of nuclei
m_j	j-th moment of the crystal size distribution
n	Nucleation rate constant
$\dot{r}_i$	Rate of reaction r_i
x	Distance from the gas-liquid interface
δ	Thickness of liquid film

1 INTRODUCTION

Precipitation generally refers to a relatively rapid formation of a sparingly soluble solid phase from a liquid solution phase (Myerson,2002). In this process supersaturation is usually generated by the addition of a third component. A chemical reaction leads to the generation of the sparingly soluble compound of interest. The resulting production rate of sparingly soluble particles is rapid since it takes place under high supersaturation conditions. In addition, due to the presence of high supersaturation, nucleation plays a major role in precipitation processes resulting in the creation of a large number of very small size particles. Since the supersaturation necessary for obtaining the crystals usually results from a chemical reaction, precipitation is often referred to as reactive crystallization (Mersmann,2001). These chemical reactions are generally very fast thus the role of the mixing and of the mass transfer of reactants is frequently important.

Industrial processes for particles precipitation can be operated in either gas or liquid phase, or in a combination of gas and liquid.

Precipitation of solids promoted by gas-liquid reactions finds application in many fields such as production of fine chemicals, biotechnology and gas cleaning but has not being extensively investigated until recently despite its industrial importance (Wachi and Jones,1995)

There is an increasing number of industrially important gas-liquid reaction systems:

- Ammonium phosphate is produced by reaction of ammonia with phosphoric acid

$$NH_{3(gas)} + H_3PO_{4(liquid)} \rightarrow NH_4PO_{4(solid)}$$

- Ammonium Sulphate is produced by production of by-product ammonia from coke ovens with sulphuric acid:

$$2NH_{3(gas)} + H_2SO_{4(liquid)} \rightarrow (NH_4)_2SO_{4(solid)}$$

  Both Ammonium sulphate and phosphate are used as fertilizers.
- Barium carbonate can be prepared by carbonation of either barium hydroxide or barium sulphate.
- Calcium carbonate is produced by the contact of carbon dioxide through a milk of lime suspension

$$Ca(OH)_{2(aq.sol)} + CO_{2(gas)} \rightarrow CaCO_{3(solid)} + H_2O$$

Precipitated calcium carbonate is widely used in chemical industries, building, agricultural and highway construction.

- Calcium sulphate is produced by gas-liquid reaction of sulphur oxide and calcium hydroxide.

These reaction systems find application in the purpose of pollution control. Sulphur dioxide present in stack gases resulting from the burning of high Sulfur coal can be removed by absorption into lime water with the precipitation of Calcium sulfate or sulfite (Wachi and Jones, 1995).

The precipitation phenomena in multiphase systems are much more complex than ones in single-phase since the intrinsic complexity of precipitation process in even influenced by interphase mass transfer. During mass transfer with chemical reaction, to create solute supersaturation and subsequent precipitation, the mass transfer often controls the overall behavior. In particular gas-liquid mass transfer phenomena determine the level of solute supersaturation and its spatial distribution in the liquid phase. In these conditions the spatial distribution of the concentration can even influence the size of the products crystals due to the high sensitivity of nucleation and crystal growth kinetics to the level of supersaturation (Wachi and Jones, 1995).

Gas-liquid precipitation processes usually involves at least three steps namely gas-liquid mass transfer, chemical reaction and crystallization.

The rates of each of these steps must to be considered to obtain a model that quantifies the phenomena that determine the crystal size distribution and predicts the rate of the whole process as a function of the design and operating parameters of the crystallization device.

This work focuses in particular on three-phase reactive crystallization in which $MgCO_3$ and $CaCO_3$ crystals are obtained by the absorption and reaction of CO_2 contained in the gas phase with a $Ca(OH)_2$ and $Mg(OH)_2$ aqueous slurries respectively.

CO_2 gas absorption into $Mg(OH)_2$ slurry is a three phase process that takes place by these following steps:

1) Dissolution of $Mg(OH)_2$ into Mg^{2+} and OH^-;
2) Absorption of CO_2 in the liquid phase which, in turn, can be seen as the result of these steps
    I. Diffusion of CO_2 gas through the gas film near the gas–liquid interface;
    II. Dissolution of CO_2 gas in the acqueous phase;
    III. Dissociation of $CO_{2(aq)}$ into bicarbonate ion (HCO_3^-);
    IV. Dissociation of $CO_{2(aq)}$ into carbonate ion (CO_3^{2-});
3) Diffusion and subsequent reactions of inorganic carbon species with Mg^{2+} within the reaction zones of the liquid film.
4) Formation of $MgCO_3$ crystals.

The reaction rate of reactive crystallization depends on the dissolution rate, absorption rate and crystallization rate jointly. Few attempts to develop towards the modeling of gas-solid-liquid reactive crystallization have been reported in literature so

far due to the complex mechanism of the process including dissolution, absorption and crystallization. The mechanism of each step is crucial to predict the whole process by combining the three models.

The purpose of this work is the development of a model for three-phase reactive precipitation in which the rate of each step of the process (dissolution, gas absorption and precipitation) is considered individually without any assumption of a rate-controlling step.

Secondly the effect of spatial non-uniformity of the concentrations of the species and of supersaturation in the liquid-film region on the kinetic of the process was analyzed. To do this the results of two different models for gas absorption and precipitation coupled with the same dissolution model were compared.

In the first one only the carbon dioxide crosses the liquid film surrounding the gas-liquid interface and both ionization reactions and precipitation occur in the bulk liquid phase only while in the second one CO_2 and all reactive ion species are assumed to move across the film by diffusional transport so that reactions and precipitation occur in the liquid film.

Since no precipitation occur in the film in the first modeling approach this will be referred to as '*Clear film model'* while the second will be referred to as '*Crystals in the film model'*.

LITERATURE PART

2 CRYSTALLIZATION

2.1 SOLUTIONS AND SOLUBILITY

In chemical engineering, crystallization is a unit operation in which a chemical compound dissolved in a solvent precipitates in controlled conditions, in order to separate it from the solvent(Mersmann,2001).

A solution is a mixture of two or more species that form a homogenous single phase. Solutions are normally thought of in terms of liquids, however, solutions may include solids suspension. Typically, the term *solution* has come to mean a liquid solution consisting a solvent, which is a liquid, and a solute, which is a solid, at the conditions of interest (Myerson,2002).

Since crystallization processes involve solutions, industrial crystallization handbooks (Mersmann,2001), (Myerson,2002), Mullin(2001),(Jones,2002) underline the importance of the knowledge of solution properties in order to the design and control the processes itself.

The maximum amount of solute that can dissolve in a given solvent is called solubility. The solubility of a substance fundamentally depends on the physical and chemical properties of the solute and solvent as well as on temperature, pressure and the pH of the solution.

The extent of the solubility of a substance in a specific solvent is measured as the saturation concentration, where adding more solute does not increase the concentration of the solution and begin to precipitate the excess amount of solute. A

saturated solution is one that is in equilibrium with excess solute present (Myerson, 2002).

The most simple case is the one in which a sparingly soluble salt (for example silver chloride) is added in water in excess of the saturation concentration. The system will eventually reach the equilibrium state and the dissociation reaction can be written as:

$$AgCl_{(S)} \leftrightarrow Ag^{+} + Cl^{-} \tag{2.1}$$

We assume that the solid is in its stable crystal form and at atmospheric pressure, we can write:

$$K_{sp} = a_{Ag^{+}} \cdot a_{Cl^{-}} = \gamma^{Ag^{+}}(m_{Ag^{+}})\gamma^{Cl^{-}}(m_{Cl^{-}}) \tag{2.2}$$

in which *m* is the concentration of ions in the solution in molal units an *γ* is the activity coefficient of the species. For sparingly soluble salts the activity coefficient can be assumed to be unity so the previous equation reduces to:

$$K_{sp} = [m_{Ag^{+}}][m_{Cl^{-}}] \tag{2.3}$$

This equation represents the solubility product of silver chloride (Myerson, 2002).

Solubility products are used to describe the solubility of sparingly soluble salts in aqueous solutions.

These relations assumes that the solutions are saturated, ideal (activity coefficient of every species equal to one) and in equilibrium and thus is an approximation except with very dilute solutions of one solute only.

The only parameter that affects the value of the solubility product (K_{PS}) of a slightly soluble salt is the temperature.

Since most solvation processes are endothermic, according to Le Châtelier's principle an increasing temperature makes the value of the K_{PS} increase and as a consequence so does the solubility.

Other factors affecting the solubility of a sparingly soluble salt are the pH of the solution and the presence in the solution of an ion common to the dissolving salt.

For concentrated solutions of electrolytes and mixture of electrolytes solubility calculation involves the calculation of the activity coefficients of the species. Many methods for calculating the activity coefficients for the ions as a function of the salt concentration are shown in ``Handbook of Aqueous Electrolyte Thermodynamics``(Guggenheim's, Bromley's, Meissner's, Pitzer's and Chen's methods)(Zemaitis et al,2010).

2.2 SUPERSATURATION, METASTABILITY AND METHODS TO CREATE SUPERSATURATION

The knowledge of solubility is important because it allows calculation of the product crystal yield that follows a change of state from a set concentration to another in which crystal forms.

Altough this mass balance is important to know the yield of the crystallization process, it does not provide any information about the rate and the time required to obtain this amount of solid. Since crystallization is a rate process, the time required for the crystallization depend on some driving force. Typically supersaturation is assumed to be the driving force of crystallization processes(Myerson, 2002).

Supersaturation is often expressed as a concentration difference:

$$\Delta c = c - c^* \tag{2.4}$$

or as a ratio of concentrations:

$$S = \frac{c}{c^*} \tag{2.5}$$

Where c is the concentration of the solution and * denotes the property at saturation (Myerson, 2002).

These two last definitions assume an ideal solution with activity coefficients of 1.

The solution to be ready for crystallization must be *supersaturated*. A solution in which the solute concentration exceeds the equilibrium (saturated) solute concentration at a given temperature is known as a supersaturated solution.

The equilibrium phase diagram plot (Miers and Isaac, 1907) provides useful informations for understanding why crystallization occurs and what type of process is suitable for production of a particular substance. It can be devided into three regions(Jones,2002).

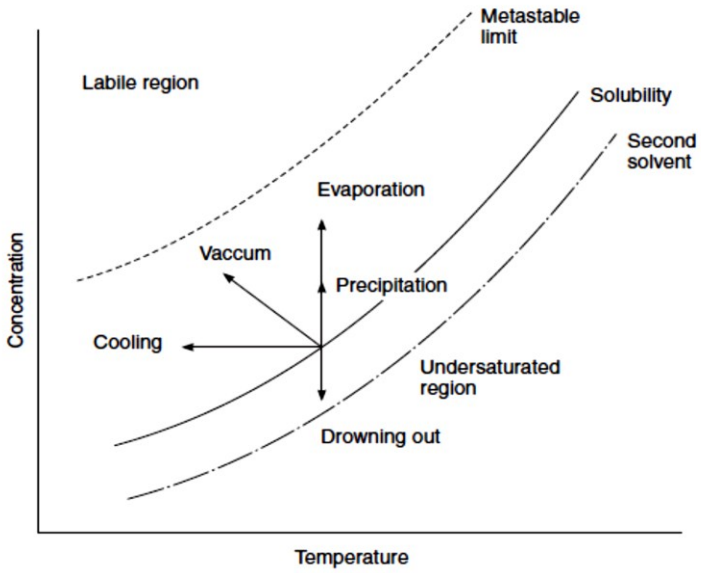

Figure 1: Solubility-supersolubility diagram (Jones, 2002)

- The stable or undersaturated zone where solute and solvent form an only homogeneous phase and crystallization is impossible
- The metastable (supersaturated) zone where spontaneous nucleation is improbable.
- The unstable or labile zone (supersaturated) where spontaneous nucleation and growth occur.

In the metastable zone the concentration of the solution exceedes the equilibrium solute concentration at the considered temperature but the solution will likely remain homogeneous. Whithin the metastable zone, however, crystal seed may grow. Every solution has a maximum amount that it can be supersaturated before becoming unstable and the solute start to precipitate immediately. The boundary that separates the unstable and the metastable zones is called *spiniodal curve.* Nevertheless the extension of the metastable zone is not always the same even considering two solutions at the same concentration of the same solute and solvent. The metastable zone width is influenced by a variety of process parameters such as rate of supersaturation generation (cooling rate or solvent's evaporation rate), impurity level, mixing and the solution history. Usually the presence of dust and dirt and a strong agitation aid the formation of nuclei and decrease the metastable zone (Jones, 2002).

Crystallization handbooks report four main methods to generate supersaturation :

- Temperature change
- Evaporation of solvent
- Chemical reaction
- Use of antisolvent

The Ostwald-Miers diagram (Fig.1) illustrates the basis of all the methods of solution growth.

2.3 CRYSTAL GROWTH FROM SOLUTIONS

Crystallization from solutions can be described as a two-step process. The first step is the 'birth' of the new crystals, the second is the growth of this crystals to larger sizes. These two processes are respectively known as nucleation and crystal growth.

The processes of nucleation and crystals growth require supersaturation. The supersaturate system then attempts to achieve thermodynamic equilibrium through nucleation and the growth of nuclei (Mersmann, 2002).

2.3.1 NUCLEATION

Nucleation can take place in a homogeneous solution that does not contain any kind of solid particles (neither foreign nor crystal of its own type) or can be facilitated if foreign particles are present. These two cases are called homogeneous and heterogeneous nucleation respectively. Both homogeneous and heterogeneous nucleation take place in absence of solution-own crystals and are collectively known as primary nucleation (Mersmann, 2002).

If crystals are present in the supersaturated solution, nucleation may occur at a lower supersaturation than needed for spontaneous nucleation and the present crystals seem to have a catalyzing effect on the nucleation phenomena (Myerson, 2002). This effect is known as secondary nucleation.

Primary nucleation generally requires high levels of supersaturation and it occurs in unseeded crystallization or precipitation.

The classical nucleation theory was developed by Wolmer(1939) and assumes of new nuclei can be described by a successive addition mechanism of units forming spherical clusters. Considering the change of free energy during homogeneous nucleation the Gibbs-Thompson relationship is obtained for describing the rate of the process:

$$B_{hom}^{0} = A_{hom} \exp\left[-\frac{16\pi\gamma^3 v^2}{3k^3T^3(\ln S)^2}\right] \quad (2.6)$$

Where S is the supersaturation ratio c/c^*.

The presence of foreign nuclei or surfaces in the solution induces heterogeneous nucleation and this phenomenon becomes significant even at low supersaturation levels. A similar relationship to can be used to describe the rate of heterogeneous nucleation:

$$B_{hom}^{0} = A_{het} \exp\left[-\frac{16\pi\gamma^3 v^2 f(\varphi)}{3k^3T^3(\ln S)^2}\right] \quad (2.7)$$

With the factor $f(\varphi)$ accounting for the decreased energy barrier due to the presence of the foreign phase.

2.3.2 CRYSTALS GROWTH

After the phase separation has begun with the nucleation process, the following stage of the crystallization process is the growth of the nuclei by the addition of solute molecules from the supersaturated solution (Myerson, 2002). This step is known as crystal growth.

Models of crystal growth describe it as a two-step process: diffusive and/or convective transfer of the units (atoms, molecules, ions) from the bulk of supersaturated solution to the surface of the growing crystal and integration in the unit in the solid phase. Supersaturation is supposed to be the driving force of the phenomenon. Since the two processes of bulk diffusion and surface reaction take place in series, the slower will control the overall rate.

Crystal growth rate is typically expressed as the rate the change in some dimension of it with time. This is called the linear grow rate and has dimension of length per unit time. Another way we can express the crystal growth rate is the mass deposition rate on the surface of the growing crystal. If *L* is a characteristic dimension of the crystal and M_C is the crystal mass we can write:

$$\frac{dM_C}{dt} = \frac{d(\rho_c f_v L^3)}{dt} = 3(\rho_c f_v L^2)\frac{dL}{dt} \qquad (2.8)$$

Where ρ_c is the crystal density and f_v is a volume shape factor assumed constant.

The entire concentration gradient $\Delta c = c - c^*$ is divided into two parts. The first, $c - c_i$ is the driving force of the convective-diffusive transport while the second $c_i - c^*$ is decisive for the integration of the unit in the growing crystal.

Therefore it is possible to express the molar flux density directed towards the crystal surface:

$$\frac{dM_C}{dt} = k_d A(c - c_i) = k_r A(c_i - c^*)^r \qquad (2.9)$$

Where k_d is the mass transfert coefficient, k_r is the reaction rate constant and *r* is the order of the reaction (Mersmann, 2001).

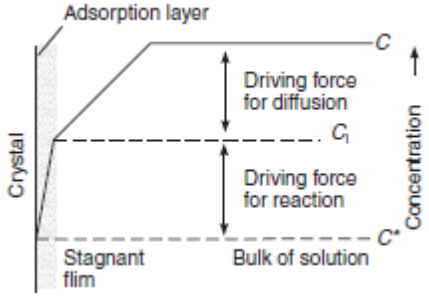

FIGURE 2: GROWING CRYSTAL-SOLUTION INTERFACE (JONES,2002)

If k_d<<k_r the growth is completely determined by diffusion and to satisfy Eq.(2.9) we have $(c - c_i\ ) \gg (\ c_i - c^*)$.

On the other hand if k_d>>k_r we have $(\ c_i - c^*) \gg (c - c_i\ )$ and the integration reaction controls the process.

If the diffusive-convective transport of units takes place rapidly or integration reaction is very slow $(k_r \to 0)$ crystal growth is determined by integration reaction on the crystal surface (Mersmann, 2001).

3 MODELING BACKGROUND OF MULTIPHASE REACTIVE CRYSTALLIZATION

While the production of $Mg(CO)_3$ by multi-phase precipitation has remained quite unexplored, the most investigated gas-liquid precipitation process in literature is the production of $Ca(CO)_3$ by absorption of CO_2 in aqueous $Ca(OH)_2$ solutions or slurries. This processes have been studied both with experimental and modeling approach.

Yagi et al. (1984) studied crystallization of $Ca(CO)_3$ by absorbing pure carbon dioxide or CO_2mixture with sulfur dioxide into aqueous solutions of calcium hydroxide. The process took place in a stirred vessel with flat gas-liquid interface. The nucleation and the growth rates were determined by the application of the mixed-slurry-mixed-product-removal reactor operating at a steady state and were related to different operating conditions. The mean size of the $Ca(CO)_3$ crystals was slightly influenced by the mean residence time and by $Ca(OH)_2$ concentration, this latter instead had a big influence on the crystal type and shape.

Kotaki and Tsuge (1990) also carried out experiments about calcium carbonate precipitation both in gas-liquid and liquid-liquid systems in a continuous MSMPR crystallizer. They investigated the effect of many operating parameters on the crystallization kinetics such as the residence time (θ), suspension density, alkalinity condition and reaction mechanism. The crystallization kinetics of calcium carbonate was described by a power law model neglecting the reaction mechanism. The growth rate was correlated as a function of the residence time (θ) and the suspension density. The kinetics orders were correlated to CO_3^{2-} alkalinity irrespective of reaction system, reaction mechanism and suspension density.

Yagi et al (1988) used a sparged stirred vessel operated as continuous for the gas and the liquid but batchwise for the sold particles with the purpose of studying the effect of the agitation rate and of the concentration of the product particle. The approach used in this studies implicitly assumes that the whole precipitation process (nucleation and growth) occurs everywhere in the liquid phase. The multiphase nature of the process, and the fact that interphase mass transfer may affect the rate of the process were not considered.

The first theory of mass transfer with reaction and precipitation was introduced by Wachi and Jones (1991a), (1991b). While each step of the process (gas- liquid mass transfer, chemical reaction and crystallization) had been investigated in depth, these authors were the first that considered the combined phenomena of the three steps on the kinetics and on the product particle characteristics. In particular they held that the non-uniformity of supersaturation in the liquid film region due to mass transfer resistance may affect the precipitation process and studied the effect of mass transfer rate on the crystal size distribution of the product partcles. In their former work (1991a) they coupled basic simultaneous equations for the film theory of gas-liquid mass transfer accompanied with chemical reaction with distributed mass and population balances for crystallization.

$$\frac{\partial A}{\partial t} = D_A\left(\frac{\partial^2 A}{\partial x^2}\right) - kAB \tag{3.1}$$

$$\frac{\partial B}{\partial t} = D_B\left(\frac{\partial^2 B}{\partial x^2}\right) - kAB \tag{3.2}$$

$$\frac{\partial C}{\partial t} = D_C\left(\frac{\partial^2 C}{\partial x^2}\right) + kAB - G' - B' \tag{3.3}$$

Where A is the gaseous reactant which is adsorbed into the solution and reacts with the liquid phase reactant B by (1-1)-order reaction. C is the sparingly soluble product which undergoes precipitation: B' and G' are the nucleation and particle growth rate respectively. While the population balance is expressed by:

$$\frac{\partial n}{\partial t} + G\frac{\partial n}{\partial L} = D_P\left(\frac{\partial^2 n}{\partial x^2}\right) \tag{3.4}$$

Figure 3 shows the conceptual concentration profiles in the liquid film region (f).

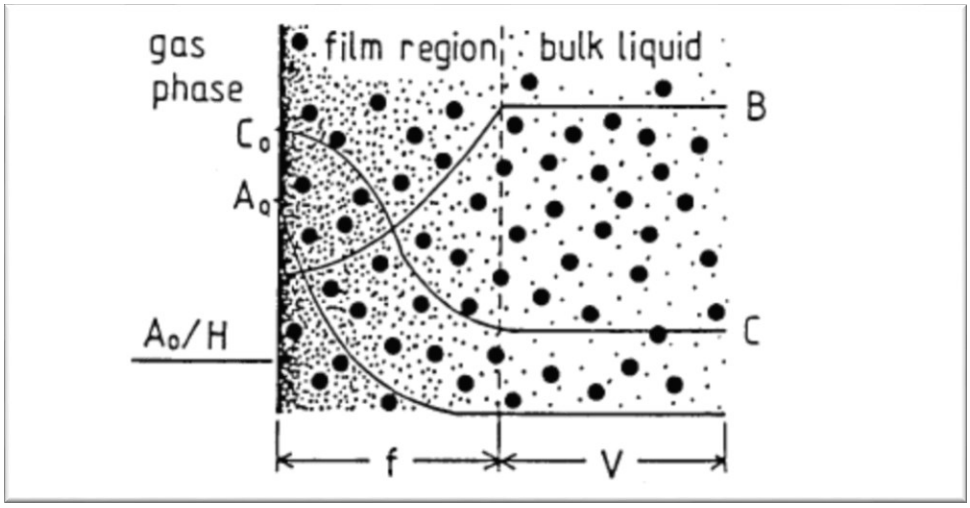

FIGURE 3: Conceptual concentration profiles in the liquid film region (Jones et al., 1992)

The model equation were applied to the precipitation of calcium carbonate resulting from absorption and chemical reaction of carbon dioxide in an aqueous calcium hydroxide using literature data and solved numerically for various hypothetical operating conditions. The resulting model predicted that at high mass transfer rates larger particles are formed especially if the reactant concentration is low; high mass transfer resistance decreases the mean crystal diameter due to accumulation of supersaturation in the liquid film. In the end even if an increasing mass transfer rate results in a rapid precipitation this lead to an increase in the induction period. The model showed good accordance with the results of the experiments carried out by Yagi et al (1984). The same authors (Wachi and Jones, 1991b) carried out experiments of batch precipitation by carbonation of lime water using a flat-interface gas-liquid agitated vessel to investigate the influence of mass transfer coefficient on the crystal size distribution. The mass transfer coefficient k_L at gas-liquid interface was expressed as a function of the stirring rate *N* with the correlation:

$$Sh = 0.322Re^{0.7}Sc^{1/3} \tag{3.5}$$

the results showed that a higher resistance of gas-liquid mass transfer led to a smaller size of the crystal confirming the predictions of the model developed in the authors' previous work.

Jones et al.(1992) carried out similar carbonation of lime water experiments in a small flat-interface reactive cell in order to investigate the effect of liquid mixing rate on the transient mean crystal size of calcium carbonate precipitated. The experimental results were compared with a model that couples mass transfer with chemical reactions and population balance equations. Like in Wachi and Jones (1991b) studies both the model and the experimental results shows the positive dependence of crystal size on the agitation rate. However while the initial mean growth rate and mixing rate dependence of the crystal size were successfully predicted by the model, the terminal crystal size was overestimated.

Tsutsumi et al. (1991) investigated the mechanism of production of calcium carbonate production injecting single gas bubbles of carbon dioxide in a calcium hydroxide solution to elucidate the role of bubble wakes in the crystallization reaction. The results of these experiments showed that small crystalline fragments are detached from the growing crystal surface to grow into new individual crystals in the wake. This means that secondary nucleation takes place in the wake due to the attrition of the growing crystals or by collision between crystals. This model of disruption leads to a bimodal distribution of particle size with many tiny particles and relatively large agglomerates.

Wachi and Jones (1992) introduced a new model for precipitation with agglomeration which describes the product particles of the process both in term of overall particle size and number of primary crystals within an agglomerate (degree of agglomeration). Inclusion of the degree of agglomeration permits the introduction in the population balance of an attrition scheme whereby a primary crystal detaches from the mother agglomerate and the evaluation of addictional particle characteristics such as surface area.

Hotomsky and Jones (1995) developed another model for gas-liquid precipitation of calcium carbonate for predicting the effect of mass transfer rate on the process in which the film theory introduced by Wachi and Jones (1991a),(1991b) was replaced by a penetration model of gas-liquid mass transfer in which the enhancement factor of CO_2 absorption was :

$$E = \frac{-D_{CO_2}\left(\frac{\partial[CO_2]}{\partial x}\right)_{x=0}}{2\cdot\sqrt{D_{CO_2}/\pi\tau}} \qquad (3.6)$$

According to this model the nucleation rate in the region next to the gas-liquid interface increases with decreasing interphase mass transfer rate while nucleation rate, particle number density and particle size show a maximum peak in position

away from the gas-liquid interface. This led to a change in the morphology and the size distribution in the wake especially during the early stage of the reaction.

Al Rashed and Jones (1999) and Rigopoulos and Jones (2001), (2003) were the first authors introducing the use of computational fluid dynamics to study the effect of the hydrodynamics on multiphase precipitators. In both the studies they considered the precipitation of $Ca(CO)_3$ via CO_2 absorption in a $Ca(OH)_2$ solution.

In the first paper Al Rashed and Jones (1999) the process was simulated in a batch precipitator with a uniform agitated gas-liquid interface similar to the device described by Wachi and Jones (1991a). A 2-D flow simulation was developed for the chemical reaction with precipitation using the moment transformation of the population balance and the Reynolds differential stress model to describe the turbulence in the system. The predictions of the CFD model were compared with the results given by the application of the film and penetration models respectively for the same time range. While film theory predicts a low variation in the mean particle size at a given time penetration theory overstimates it. The CFD simulation predicted an intermediate performance giving results closer to the ones observed experimentally.

In the second study Rigopoulos and Jones (2001) the authors developed a model for a bubble column reactor with solid particle precipitation. First a CFD model of the bubble reactor was built in order to predict hydrodynamic variables of the system such as gas hold-up and liquid circulation. The penetration theory of gas-liquid absorption was integrated into a reaction engineering model that accounts for the different reaction environments emerging in the bulk and the interface by the use of two different forms of the population balance for the prediction of the particle size evolution. The model was applied to the precipitation of $Ca(CO)_3$ by absorption of CO_2. In particular the same precipitation device studied by Hotomsky and Jones

(1995) was simulated under the same operating conditions in order to compare experimental data with the model predictions.

With a similar approach the gas-liquid precipitation of calcium carbonate was modeled by the same authors in bubble column reactor taking even in account the agglomeration phenomenon (Rigopoulos and Jones, 2003).

Cournil and Herri (2003) revisited the problem of gas-liquid reactive crystallization using a two-film model to describe the gas-liquid mass transfer rate. Coupling it with kinetic model for chemical reactions, equations for the distributed crystal population and crystallization kinetic laws they obtained the typical partial derivative equation problem for the description of the process. In particular the role of the interfacial film in the growth of the crystals depending on the size of the considered crystal was clarified. However, the formulation obtained in terms of moments of the crystal size distribution was not solved numerically as the previous author did. The authors proposed a new procedure to obtain the asymptotic laws,that describes the time dependence of crystal number and size, in an analytical form in which the effect of operating parameters are explicitly expressed.

Kakaranija and Mehra (2007) stated that the film model used by Wachi and Jones (2002) for the description of the gas-liquid mass transfer showed some conceptual problems since:

- it does not take in account the convective mixing occurring between the interfacial film and the bulk for larger particles that, according to the Stockes-Einstein equation, have low diffusivity.

- makes no distinction between the time of the batch process and the time liquid elements spend at the gas liquid interface.

Therefore Kakaranija and Mehra (2007) stated that a mass transfer model, that explicitly accounts the convective exchange of liquid between bulk and gas-liquid

interface, would be more appropriate to describe a system in which particles in the micrometer size range are formed. They adopted, for gas-liquid mass transfer, the penetration model of Higbie like in Hotomsky and Jones (1995) work. Their model filled some gaps of Hotomsky and Jones (1995) study such as the lack of information about the crystal size distribution, the negligence of the effect of particle diffusivity and some inconsistencies in the boundary conditions. In addition the model predictions were compared with experimental data of a $Ca(OH)_2 - CO_2 - H_2O$ precipitation system.

Lin et al (2006) investigated the influence mass transfer on reactive multiphase crystallization by an experimental study of calcite precipitation in a $Na_5P_3O_{10} - Ca(OH)_2 - CO_2 - H_2O$ system. The main difference between this study and the previous ones is the fact that the calcium hydroxide is not completely dissolved in water but is suspended in form of particle forming a reactive slurry. In this configuration a new step, dissolution of the calcium hydroxyl, is introduced in the process and may control the rate of the precipitation. The kinetics of the system were evaluated comparing the rate of calcium hydroxyl dissolution, carbon dioxide absorption and calcium carbonate precipitation. The experimental results showed that the rate controlling step shifts from crystallization of calcite to calcium hydroxyl dissolution at a turning time θ_C while the transfer resistance for carbon dioxide absorption was negligible during the whole reaction time.

Recently several experimental studies concerning precipitation of magnesium carbonate ($MgCO_3$) from a reaction of magnesium hydroxide ($Mg(OH)_2$ suspension and CO_2 underlined both the role of gas-liquid mass transfer and the kinetic of the $Mg(OH)_2$ on the rate of $MgCO_3$precipitation. Since previous studies (Vermilyea, 1969), (Pokrovsky et al. 2004) concluded that $Mg(OH)_2$ dissolution is mostly surface controlled, Hövelmann et al. (2012) assumed that both dissolution and precipitation are controlled by the $MgOH_2^+$ surface species. Experimental data confirmed the assumption since more abundant nucleating particles were obtained at lower pH

indicating that brucite carbonation is rate limited by the release of Mg^{2+} ion from the dissolving surface. Han et al. (2014) carried out experiments of $MgCO_3$ precipitation from a reaction of $Mg(OH)_2$ and CO_2 in a semi-batch reactor with different mixing speed and CO_2 flow rates at ambient temperature and pressure. The precipitation kinetics was determined by pH measurements and the pH evolution were compared to $CaCO_3$ precipitation. The results showed that the precipitation of $CaCO_3$ was much faster than $MgCO_3$. This happen because the solubility of $Ca(OH)_2$ is hundred times higher than that of $Mg(OH)_2$. Shifting the mixing rate from 560 rpm to 650 rpm the pH values dropped faster due to the promotion of $Mg(OH)_2$ at higher turbulence conditions. A further increase in the stirring rate did not make the pH fall any faster indicating that, in these conditions, the mass transfer of $CO_2$is the kinetic controlling step.

These results clearly show that, in the case the reactive crystallization involves three different phases (solid reactant particles, aqueous phase of the slurry and gas phase) even the dissolution rate of the suspended particles can be the rate determining step of the whole precipitation process in addition to the kinetic of gas-liquid mass transfer and of the product particle birth and growth.

Therefore the development of a holistic model for three-phase precipitation, suitable in different operating conditions, must involve the modeling of each of the step of the process: solid-liquid mass transfer (dissolution), gas-liquid mass transfer (absorption) and crystallization.

While previous studies focused on the modeling of reactive precipitation by absorption of gas in homogeneous solutions, the purpose of this study in to include a kinetic model for the Magnesium and Calcium hydroxide dissolution in an holistic model for $MgCO_3$ and $CaCO_3$ precipitation processes by absorption of CO_2 into a $Mg(OH)_2$ and $Ca(OH)_2$ aqueous suspension respectively.

4 MODELING BACKGROUND OF PARTICLES DISSOLUTION

The earliest dissolution experiments were carried out by Noyes and Whitney (1897). They studied the dissolution rate of sparingly soluble compounds finding out that this is proportional to the difference between the instantaneous concentration and the saturation solubility:

$$\frac{dC_b}{dt} = k_d(C_s - C_b) \tag{4.1}$$

The simplest model for predicting the interfacial mass transfer was proposed by Nernst in 1904. This model was developed for gas-liquid interfaces but gives good results even for solid-fluid interfaces and assumes that a stagnant film exist near every interface (δ)(Sherwood et. al 1974). Nernst showed that k_d is a composite constant and is a linear function of the diffusion coefficient and the external area of the dissolving body:

$$\frac{dC_b}{dt} = \frac{D_C S}{V \cdot \delta} \tag{4.2}$$

According to it the flux of solvent toward the bulk solution can be calculated in term of mass transfer coefficient and the difference between the interfacial concentration of the solute and its concentration in the bulk solution. However this model assumes that the concentration of solute in the bulk liquid phase is constant, so it can be applied only for the case of low solubility.

These equations are used when the rate of mass transfer in the layer surrounding the particle is slower than the reaction at the solid-liquid interface.

Applying this model and using a rotating disk device, Levich (1962) developed an explicit relationship between the agitation rate and the thickness of the stagnant film and the agitation rate.

Chen and Wang (1989) showed that the film model and the assumption of pseudo-steady state is suitable for the case of low solubility solids and proposed a more accurate model for the dissolution rate for the characterization of the dissolution of spherical solid particles in a stagnant fluid.

Bhaskarwar (1988) analyzed the dissolution of mono-disperse solid particles obtaining a model in which the mass transfer coefficient varies with the size of the dissolving particle. Even in this study the transient nature of the dissolution process is taken into account and brought to non-linear ordinary differential equations that were solved by rigorous numerical methods.

Assuming that the dissolving particles are spherical, the dissolution rate can be defined by a ”Shrinking core model”. In this case only the solubility of only one of the components contained in the solid phase is appreciable compared with the rest of the components. If the amount of the dissolving component is limited, the appearance and the size of the solid particles will remain essentially the same during the course of dissolution (Hsu et al, 2009). The zone of the reaction moves into solid leaving behind completely converted material and inert solid. Thus at any time there exist an unreacted core of material which shrinks in size during the reaction (Levenspiel, 1999). As dissolution proceeds, the undissolvable solid phase provides a resistance for diffusion of solute molecules towards the bulk liquid phase. Therefore the dissolution of the solute consists of many steps:

- Diffusion reactant in the liquid phase through the film surrounding the particle to the surface of the solid.
- Penetration and diffusion of the reactant through the blanket of ash to the surface of the unreacted core.

- Reaction of with solid at this reaction surface.
- Diffusion of products through the ash back to the exterior surface of the solid
- Diffusion of products through the gas film back into the main body of fluid.

Assuming that the concentration of the solute on the solid-solid interface is at saturation we obtain:

$$\frac{\partial C}{\partial t} = \frac{D_1}{r^2}\frac{\partial}{\partial r}\left(r^2\frac{\partial C}{\partial r}\right) \ , \quad r_c < r < r_0 \tag{4.3}$$

$$\frac{\partial C}{\partial t} = \frac{D_2}{r^2}\frac{\partial}{\partial r}\left(r^2\frac{\partial C}{\partial r}\right) \ , r_0 < r < r_0 + \delta \tag{4.4}$$

Where D_1 and D_2 are respectively the effective diffusivity of solute in the solute free solid phase and the diffusivity of solute in the surface layer, r_c and r_0 are the radius of the particle and the radius of the core and δ is the thickness of the surface layer.

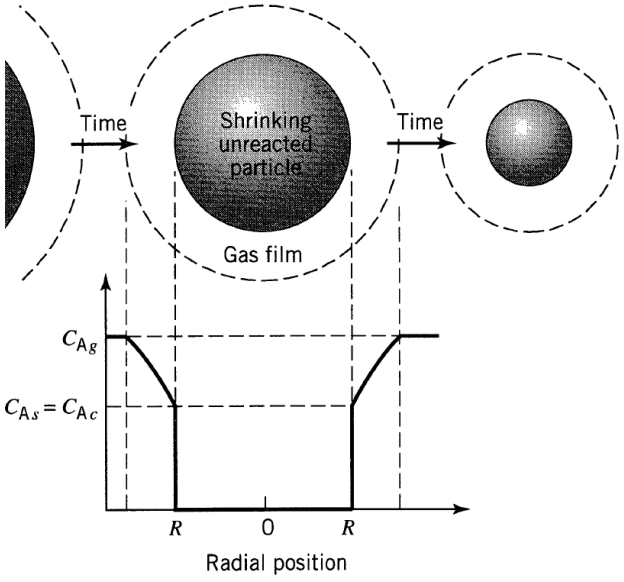

FIGURE 4: REPRESENTATION OF CONCENTRATION OF REACTANTS AND PRODUCTS FOR THE REACTION $A_{(fluid)} + bB_{(solid)} \leftrightarrow rR_{(fluid)}$ BETWEEN A SHRINKING PARTICLE AND FLUID. (LEVENSPIEL, 1999)

Hsu et al. (2009) and Levenspiel (1999) solved these equations obtaining an expression of the dissolution rate in many conditions:

- Constant bulk concentration;
- Variable bulk concentration;
- Solid phase diffusion controls;
- Chemical reaction controls;
- Surface layer diffusion controls;

Solutions can be found even in the case than no ash forms and the particle shrinks during the reaction finally disappearing (Hsu et al, 2009).

Several studies about the dissolution rate of $Mg(OH)_2$ in aqueous solutions can be found in literature.

Vermileyea (1969) studied the dissolution rates of natural Brucite, optical grade MgO and commercial $Mg(OH)_2$ suspending 10-30μ diameter powders in a $10^{-1}M\ KCl$ slowly stirred solution. The initial pH of the solution was about 3 and the dissolution rate was computed from the rate of change of the pH which rose as the powder dissolved. The results of the experiments indicates that the dissolution mechanism involves a surface reaction between hydroxyl ions and protons. For pH lower than 5 this surface reaction is rate-determining and the rate increases as the square root of the proton concentration. Above pH 5 the proton arrival is the slow rate-determining step.

Pokrovsky (2004) studied the dissolution and precipitation rates of natural $Mg(OH)_2$ (Brucite) at 25°C as a function of pH, ionic strength, saturation index and aqueous magnesium concentration. A surface speciation model was used to describe the brucite surface charge and to model brucite's dissolution kinetics. It is assumed that the surface hydroxyl groups are ampholytes and undergo protonation/deprotonation reactions. According to this model three species were postulated to exist on the

water-brucite interface: $MgOH_2^+$, $MgOH^0$ and MgO^-. $MgOH_2^+$ is predicted to be the dominant species at pH<8 while it is progressively replaced by $MgOH^0$ and MgO^- as pH increases to 10-12. Rates were found to be proportional to the square of $MgOH_2^+$ and independent on the ionic strength of the solution. The rate equation

$$R = k_{Mg}^{+}[MgOH_2^+]^2(1-\Omega^2)$$

describes brucite dissolution kinetics over a wide range of solute composition.

Bharadway et al (2013) studied the dissolution rate of $Mg(OH)_2$ by HCl titration in order to study the dissolution's kinetic of this compound. The rate of release of magnesium and hydroxyl ions is indeed a crucial step in the $Mg(OH)_2$-absorption process by reactive crystallization. The dissolution rate was computed by correlating it to the rate of HCl required to maintain the pH at a preset value. The experiment took place at different temperatures, mixing rates and pHs and in all of them magnesium hydroxide powder with average particle size of 6μm was added in water to obtain a 0.01M solution. The average particle size was periodically measured during the experiment. The dissolution process was found to be controlled by surface reaction between $Mg(OH)_2$ and H^+ since the dissolution rate showed an exponential dependence on the temperature. The dissolution was modeled with a shrinking core model in which the surface reaction is the rate-controlling step. An intrinsic kinetic was determined from the model and succeeded in predicting the particle size during the process. Finally the order of the surface reaction was estimated to be 0.20-0.31 and this probably means that

$$Mg(OH)_2 + 2\,HCl \rightarrow MgCl_2 + 2H_2O$$

Is not an elementary reaction but likely takes place via formation of magnesium-complexes on the surface.

APPLIED PART

The purpose of this work is the development and the comparison of two different models for three-phase reactive precipitation by coupling kinetic equations for gas-liquid absorption, particles dissolution and crystallization.

The operational conditions implemented in the model were the one described by Han et al. (2014).

Their study focused on the investigation of the kinetics of precipitation of $MgCO_3$ and $CaCO_3$ from the reaction of $Mg(OH)_2$ and $Ca(OH)_2$ particles, suspended in water, and CO_2.

Experiments were carried out in a 3-L capacity glass reactor equipped with a Rushton turbine and a gas sparger located at the bottom of the reactor for bubbling pure CO_2 into a 3.8 wt % suspension of $Mg(OH)_2$ and $Ca(OH)_2$ respectively.

The experiments were carried out at different stirring and gas flow rates for investigating the influence of the mass transfer on the precipitation process.

Two different models for gas-liquid mass transfer and precipitation were coupled with a model for particle dissolution in order to obtain a holistic model for predicting the kinetics of three-phase precipitation processes.

5 DESCRIPTION OF THE MODELS

5.1 DISSOLUTION MODEL

The model adopted for describing the dissolution rate of the $Mg(OH)_2$ and $Ca(OH)_2$ particles in the slurry is a "Shrinking particle model" for spherical and nonporous particles (Levenspiel, 1999).

Assuming that all the particles loaded in the system have a spherical geometry and the same initial radius the dissolution is supposed to proceed from the outer skin of the spherical particle towards the center of it with the particle shrinking during the dissolution and finally disappearing. The particles are assumed to be pure $Mg(OH)_2$ or $Ca(OH)_2$ and no inert solid is left while the dissolution proceeds.

The reaction considered is the following:

$$Mg(OH)_2(s) \leftrightarrow Mg^{2+} + 2OH^- \quad (5.1)$$

Assuming that the diffusion of hydroxyl ions away from the solid-liquid interface through the liquid film surrounding the particle is the rate limiting step for the process, the molar flux of OH^-that dissolve from the solid's surface to the bulk liquid can be expressed as follow:

$$N_{OH^-} = k_s(C_{OH^-(i)} - C_{OH^-(b)}) \quad (5.2)$$

Where $C_{OH^-(i)}$ is the concentration of OH^- at the solid-liquid interface, while $C_{OH^-(b)}$ denotes the concentration of OH^- in the bulk liquid phase of the slurry and k_s is the solid-liquid mass transfer coefficient.

The molar flux of Mg^{2+}, considering the stoichiometry of the reaction, is:

$$N_{Mg^{2+}} = \frac{1}{2} N_{OH^-} \tag{5.3}$$

$C_{OH^-(i)}$ is constant and assumed to be the equilibrium concentration in the liquid phase of a $Mg(OH)_2$ aqueous suspension at the operational temperature. If K_{SP} is the solubility product of $Mg(OH)_2$ we have:

$$K_{SP(Mg(OH)_2} = \left(C_{OH^-(i)}\right)^2 C_{Mg^{2+}(i)} \tag{5.4}$$

$$C_{OH^-(i)} = 2C_{Mg^{2+}(i)} \tag{5.5}$$

$$C_{OH^-(i)} = \sqrt[3]{\frac{K_{SP(Mg(OH)_2)}}{4}} \tag{5.6}$$

The time course of the concentration of Mg^{2+} and OH^- in the bulk liquid phase can be expressed as follow:

$$\frac{dC_{Mg^{2+}}}{dt} = a_s N_{Mg^{2+}} \tag{5.7}$$

$$\frac{dC_{OH^-(b)}}{dt} = a_s N_{OH^-} = k_s a_s (C_{OH^-(i)} - C_{OH^-(b)}) \tag{5.8}$$

$a_s$is the specific surface area for the solid- liquid mass transfer, i.e the total solid-liquid surface area per unit of bulk volume. Assuming that the volume of

the solid phase in the slurry is negligible compared to the volume of the liquid phase a_S can be expressed as follow:

$$a_S = \frac{A_{tot}}{V_{liquid}} \tag{5.9}$$

A_{tot} is the total solid-liquid contact area of the suspension and assuming that the total number of dissolving particles N_{tot} in the system is constant and have the same size and spherical shape:

$$A_{tot} = N_{tot}\pi d_P^2 \tag{5.10}$$

In which d_P is the time dependent diameter of the dissolving shrinking particles.

Coupling equation (5.9) and (5.10) we can express the specific surface area a_s as a function of the diameter d_P of the shrinking particle:

$$a_S = \frac{N_{tot}\pi d_P^2}{V_{liquid}} \tag{5.11}$$

The mass of dissolving solid Magnesium hydroxide $m_{Mg(OH)_2}$ can be expressed as:

$$m_{Mg(OH)_2} = \frac{4}{3}\pi\left(\frac{d_P}{2}\right)^3 N_{tot}\rho_{Mg(OH)_2} = \frac{\pi {d_P}^3 N_{tot}\rho_{Mg(OH)_2}}{6} \tag{5.12}$$

By solving equation (5.11) for particle diameter we have:

$$d_P = \sqrt{\frac{a_S V_{liquid}}{\pi N_{tot}}} \tag{5.13}$$

and substituting in eq. (5.13) we obtain an explicit correlation between the specific surface area a_s and the mass of solid $Mg(OH)_2$ present in the system.

$$a_s = \left(\frac{6\pi^{1/2} {N_{tot}}^{1/2} m_{Mg(OH)_2}}{\rho_{Mg(OH)_2} {V_{liquid}}^{3/2}} \right)^{3/2} \qquad (5.14)$$

Now we have explicit correlations between the value of the specific surface area of the system and the time dependent value of the particle diameter d_P or the total mass $m_{Mg(OH)_2}$ of the dissolving particles, as a consequence even the value of a_s will not be constant during the process but will decrease during it reaching the zero value when all the particles are completely dissolved ($d_P = 0 \ \ or \ m_{Mg(OH)_2} = 0$).

On the other hand even the value of the solid-liquid mass transfer coefficient k_s cannot be assumed constant during the evolution of the dissolution process since the film resistance at the surface of a particle depends on numerous factors such as the relative velocity between particle and fluid, the fluid properties and the size of particles (Levenspiel,1999) .Assuming well mixed conditions in the system and that the dissolution process does not affect the properties of the liquid phase (i.e. viscosity, or temperature) the only parameter that will affect the time evolution of the value of k_s is the size d_P of the dissolving particles. The mass transfer coefficient was calculated using the correlation proposed by Asai et al. (1989) for agitated gas-liquid-solid system with sparged gas and fine solid particles suspended:

$$Sh = \left\{ 2^{5.8} + \left[0.61 \left(\frac{\varepsilon_T^{1/3} d_P^{4/3}}{\nu} \right) Sc^{1/3} \right]^{5.8} \right\}^{1/5.8} \qquad (5.15)$$

Where ν is the kinematic viscosity of liquid, d_P is the particle diameter while Sc and Sh are respectively the dimensionless Schmidt and Sherwood numbers:

$$Sc = \frac{\nu}{D_{OH^-}} \tag{5.16}$$

$$Sh = \frac{k_s d_P}{D_{OH^-}} \tag{5.17}$$

Where D_{OH^-} is the diffusion coefficient of hydroxyl ions.

ε_T in equation (5.15) is the total energy dissipation rate which in turn is the sum of the energy dissipation rate due to the mechanical agitation ε_M and the energy dissipation rate due to the sparged gas ε_G(Asai et al.,1989) .

$$\varepsilon_T = \varepsilon_M + \varepsilon_G \tag{5.18}$$

The first term of equation (5.18) can be estimated as in Garcia-Ochoa and Gomez (2004):

$$\varepsilon_M = \frac{P}{\rho(\pi/4)T^2 H} \tag{5.19}$$

Where P is the power input under gassed conditions, ρ is the density of the slurry while T and H are respectively the stirrer's diameter and height.

Power consumption in aerated systems (P) can be expressed as a function of power consumption in un-aerated systems (P_0) according to the correlation proposed by Michel and Miller (1962):

$$P = \alpha \left(\frac{P_0^2 N T^3}{Q^{0.56}}\right)^{\beta} \tag{5.20}$$

Where N is the stirring speed, Q is the gas flow rate and α and β are two constants depending on the stirrer type and system configuration (Garcia-Ochoa and Gomez, 2004).

P_0 can be evaluated using the power number N_P which again is a constant depending on the impeller type and geometry (Garcia-Ochoa and Gomez, 2004):

$$P_0 = N_P \rho N^3 T^5 \quad (5.21)$$

The second term in equation (5.18) ε_G is evaluated as in Asai et al. (1989):

$$\varepsilon_G \approx U_G g \quad (5.22)$$

where U_G is the superficial gas velocity and g is the acceleration of gravity.

5.2 ABSORPTION MODEL AND CRYSTALLIZATION MODELS

When CO_2 dissolves into aqueous solutions ionization reactions occur leading to the formation of carbonate (CO_3^{2-}) and bicarbonate (HCO_3^-) ions.

The reactions involved are the following:

$$r_1: \quad CO_2(l) + OH^- \overset{k_{11}/k_{12}}{\longleftrightarrow} HCO_3^- \tag{6.1}$$

$$r_2: \quad HCO_3^- + OH^- \overset{k_{21}/k_{22}}{\longleftrightarrow} CO_3^{2-} + H_2O \tag{6.2}$$

$$r_3: \quad H^+ + OH^- \overset{k_{31}/k_{32}}{\longleftrightarrow} H_2O \tag{6.3}$$

$$r_4: \quad CO_2(l) + H_2O \overset{k_{41}/k_{42}}{\longleftrightarrow} HCO_3^- + H^+ \tag{6.4}$$

Where k_{i1} and k_{i2} are respectively the kinetic constants for the direct and reverse reaction r_i.

The rate of each reaction can be calculated as a function of the reaction kinetic constants and the concentration of the reactants as follow:

$$\dot{r_1} = k_{11} C_{CO_2(l)} C_{OH^-} - k_{12} C_{HCO_3^-} \tag{6.5}$$

$$\dot{r_2} = k_{21} C_{HCO_3^-} C_{OH^-} - k_{22} C_{CO_3^{2-}} \tag{6.6}$$

$$\dot{r_3} = k_{31} C_{H^+} C_{OH^-} - k_{32} \tag{6.7}$$

$$\dot{r_4} = k_{41} C_{CO_2(l)} - k_{42} C_{HCO_3^-} C_{H^+} \tag{6.8}$$

Carbonate ions CO_3^{2-} generated by reaction r_2 will react with magnesium ions resulting from the dissolution of $Mg(OH)_2$ particles in the slurry according to the reaction:

$$Mg^{2+} + CO_3^{2-} \rightarrow MgCO_3(s) \quad (6.9)$$

which is not a simple homogeneous reaction but involves the precipitation of solid $MgCO_3$ crystals.

As a consequence the kinetic modelling of reaction 6.9 involves the use of a kinetic model for nucleation and growth rate of growing crystals depending on the transient supersaturation in the liquid phase of the three-phase system which, in turn, is dependent on the dissolution rate of the $Mg(OH)_2$particles and on the rate and the rate of CO_3^{2-} production by r_2.

In addition one more kinetic model is needed for determining the rate of CO_2 absorption in the liquid phase of the slurry. Absorption of CO_2 in liquid phase:

$$CO_2(g) \rightarrow CO_2(l) \quad (6.10)$$

involves gas-liquid mass transfer. Thus a mass transfer kinetic model is necessary for calculating the transient concentration of dissolved carbon dioxide $CO_2(l)$ which is necessary for estimate the rate of reactions r_1 and r_4.

5.2.1 CLEAR FILM MODEL

In this modeling approach we assume that the kinetics of the reactions and crystallization in the diffusion layer surrounding the gas-liquid interface is slow and can be neglected.

With this assumption the gas absorption will occur through a clear liquid film and reactions r_1, r_2, r_3, r_4 and $MgCO_3$ precipitation will occur in the bulk only (Wachi and Jones ,2002).

Assuming that the resistance to mass transfer in the gas phase is negligible we have:

$$\frac{dC_{CO_{2(l)}}}{dt} = k_L a_L (C_{CO_{2(l)}(i)} - C_{CO_{2(l)}}) \tag{6.11}$$

where $C_{CO_{2(l)}(i)}$ is the concentration of dissolved CO_2 at the gas-liquid interface, $C_{CO_{2(l)}}$ is the concentration of dissolved CO_2 in the bulk liquid phase, k_L gas-liquid mass transfer coefficient and a_L is the specific surface area for gas liquid mass transfer.

Assuming that at the gas-liquid interface the concentration of dissolved CO_2 is the equilibrium concentration we can write:

$$C_{CO_{2(l)}(i)} = p_{CO_2} H \tag{6.12}$$

where p_{CO_2} is the partial pressure of CO_2 in the gas phase, and H is the Henry's constant.

For the calculation of k_L and $a_l$method proposed by Garcia-Ochoa and Gomez (2004) was adopted:

$$k_L = \frac{2}{\sqrt{\pi}}\sqrt{D_L}\left(\frac{\varepsilon\rho}{\mu}\right)^{1/4} \quad (6.13)$$

Where D_L is the diffusivity coefficient of the component (CO_2in our case) in the liquid, ρ and μ are respectively the density and dynamic viscosity of the liquid while ε is calculated as in equation (5.18).

The specific surface area was calculated a_l as a function of the gas hold-up ϕ and the average diameter of the bubbles d_b:

$$a_L = \frac{6\phi}{d_b} \quad (6.14)$$

For the calculation of the gas hold-up and average bubble size Garcia-Ochoa and Gomez (2004) proposed the equations derived by Kudrewizki et al. (1986) and Bhavaraju (1978) respectively:

$$\frac{\phi}{1+\phi} = 0.819\frac{V_S^{2/3}N^{2/5}T^{4/15}}{g^{1/3}}\left(\frac{\rho_L}{\sigma}\right)^{1/5}\left(\frac{\rho_L}{\rho_L-\rho_G}\right)\left(\frac{\rho_L}{\rho_G}\right)^{-1/15} \quad (6.15)$$

$$d_b = 0.7\frac{\sigma^{0.6}}{(P/V)^{0.4}\rho_L^{0.2}}\left(\frac{\mu_L}{\mu_G}\right)^{0.1} \quad (6.16)$$

Where V_S is the superficial gas velocity, N is the stirring rate, T the impeller's diameter, σ the interfacial tension while P and V are the power input under gassed conditions and the volume of liquid in the tank respectively.

After setting a mathematical model for the kinetic of absorption of CO_2 in the liquid phase the calculation of the time evolution of the concentrations of the species involved in reactions r_1, r_2, r_3, r_4 can be calculated:

$$\frac{dC_{CO_{2(l)}}}{dt} = k_l a_l \left(C_{CO_{2(l)}(i)} - C_{CO_{2(l)}} \right) - \dot{r_1} - \dot{r_4} \tag{6.17}$$

$$\frac{dC_{OH^-}}{dt} = -\dot{r_1} - \dot{r_2} - \dot{r_3} \tag{6.18}$$

$$\frac{dC_{H^+}}{dt} = -\dot{r_3} + \dot{r_4} \tag{6.19}$$

$$\frac{dC_{HCO_3^-}}{dt} = \dot{r_1} - \dot{r_2} + \dot{r_4} \tag{6.20}$$

$$\frac{dC_{CO_3^{2-}}}{dt} = \dot{r_2} \tag{6.21}$$

This is the case of absorption of CO_2 in pure water. In our system one more reactant, Mg^{2+}, is in the liquid phase due to the dissolution of $Mg(OH)_2$ particles. Magnesium ions will react with CO_3^{2-} resulting in $MgCO_3$ crystals precipitation according to reaction (6.9).

For the calculation of the kinetics of crystallization kinetics, the number rate of nucleation B and growth rate were expressed as a power-law function of supersaturation like in Wachi and Jones (1992):

$$B = k_n(S)^n \tag{6.22}$$

$$G = k_g(S)^g \tag{6.23}$$

Supersaturation S is calculated like in Wachi and Jones (1992):

$$S = \sqrt{C_{CO_3^{2-}} C_{Mg^{2+}}} - \sqrt{K_{sp}} \tag{6.24}$$

Where K_{sp} is the solubility product of $MgCO_3$.

Assuming ideal mixing conditions in the bulk liquid phase, neglecting aggregation and breakage phenomena the population balance can be expressed as in Hotomsky and Jones (1995):

$$\frac{\partial n(t,L)}{\partial t} + \frac{\partial (Gn(t,L))}{\partial L} = 0 \tag{6.25}$$

Assuming then a size-independent growing rate:

$$\frac{\partial n(t,L)}{\partial t} + G\frac{\partial n(t,L)}{\partial L} = 0 \tag{6.26}$$

In order to solve the equation, the moment transformation method of the population balance was adopted as in Wachi and Jones (1992). The j-th moment m_j of the density distribution is defined as:

$$m_j(t) = \int_0^\infty n(t,L)L^j dL \tag{6.27}$$

and the time evolution of the moments can be expressed as:

$$\frac{dm_j}{dt} = jGm_{j-1} + BL_0^j \tag{6.28}$$

Where $L_0$is the effective nucleic diameter.

The molar precipitation rate per unit volume of solid $MgCO_3$ can be expressed as in Wachi and Jones (1992):

$$\dot{r}_{MgCO_3} = \frac{G}{2} m_2 \rho\beta + \alpha\rho BL_0^3 \tag{6.29}$$

Where ρ is the molar density of solid $MgCO_3$ while α and β are respectively the volume to length shape factor and the surface to length shape factor.

Assuming that the precipitated particles are spherical we have $\alpha = \pi/6$ and $\beta = \pi$ (Wachi and Jones, 1992).

The mass precipitation rate can be expressed as:

$$\dot{m}_{MgCO_3} = \dot{r}_{MgCO_3} M_{MgCO_3} V_S \tag{6.30}$$

where M_{MgCO_3} and V_S are respectively the molar mass of $MgCO_3$ and the volume of the slurry.

Now that mathematical models are set for dissolution, absorption and crystallization rates it is possible to combine them to obtain a system of ordinary differential equation for describing then time evolution of all the chemical species involved in the process in the well mixed bulk liquid phase.

$$\frac{dC_{CO_{2(l)}}}{dt} = k_L a_L \left(C_{CO_{2(l)}(i)} - C_{CO_{2(l)}} \right) - \dot{r_1} - \dot{r_4} \tag{6.31}$$

$$\frac{dC_{OH^-}}{dt} = -\dot{r_1} - \dot{r_2} - \dot{r_3} + a_s N_{OH^-} \quad (6.32)$$

$$\frac{dC_{H^+}}{dt} = -\dot{r_3} + \dot{r_4} \quad (6.33)$$

$$\frac{dC_{HCO_3^-}}{dt} = \dot{r_1} - \dot{r_2} + \dot{r_4} \quad (6.34)$$

$$\frac{dC_{CO_3^{2-}}}{dt} = \dot{r_2} - \dot{r}_{MgCO_3} \quad (6.35)$$

$$\frac{dC_{Mg^{2+}}}{dt} = a_s N_{Mg^{2+}} - \dot{r}_{MgCO_3} \quad (6.36)$$

$$\frac{dm_0}{dt} = B \quad (6.37)$$

$$\frac{dm_1}{dt} = Gm_0 + BL_0 \quad (6.38)$$

$$\frac{dm_2}{dt} = 2Gm_1 + BL_0^2 \quad (6.39)$$

$$\frac{dm_3}{dt} = 3Gm_2 + BL_0^3 \quad (6.40)$$

The initial conditions were implemented assuming that, at the beginning of the process, the dissolving particles of $Mg(OH)_2$ are at equilibrium with the liquid phase. Thus the liquid phase is a saturated $Mg(OH)_2$solution.

$$K_{SP(Mg(OH)_2} = \left(C_{OH^-(t=0)}\right)^2 C_{Mg^{2+}(t=0)} \quad (6.41)$$

$$C_{OH^-(t=0)} = \sqrt[3]{\frac{K_{SP(Mg(OH)_2)}}{4}} \quad (6.42)$$

$$C_{Mg^{2+}(t=0)} = \frac{1}{2} C_{OH^-(t=0)} \tag{6.43}$$

If the concentrations of ionic species are expressed in mol/m^3 the initial concentration of H^+can be calculated as:

$$C_{H^+(t=0)} = \frac{10^{\left(pK_W + log\left(\frac{C_{OH^-(t=0)}}{1000}\right)\right)}}{1000} \tag{6.44}$$

Since the bubbling of CO_2 in the slurry occurs for $t > 0$, at the initial time no carbon dioxide, carbonate and bicarbonate ion are dissolved in the liquid phase.

$$C_{CO_{2(l)}(t=0)} = 0 \tag{6.45}$$

$$C_{HCO_{3(t=0)}^-} = 0 \tag{6.46}$$

$$C_{CO_3^{2-}(t=0)} = 0 \tag{6.47}$$

As a consequence no $MgCO_3$ crystals are in the slurry:

$$n(t = 0, L) = 0 \tag{6.48}$$

Thus, from equation (6.27):

$$m_j(t = 0) = 0 \tag{6.49}$$

5.2.2 CRYSTALS IN THE FILM MODELS

5.2.2.1 STAGNANT CRYSTALS IN THE FILM MODEL

In this modeling approach both reactions r_1, r_2, r_3, r_4 and crystallization are assumed to occur in the liquid film surrounding the gas bubbles and the bulk liquid phase of the slurry. We keep in account here the mass transfer due to diffusional transport of each species across the film.

The length of the film δ was calculated as:

$$\delta = \frac{D_{CO_2}}{k_L} \tag{6.50}$$

Where D_{CO_2} is the diffusivity coefficient of absorbed CO_2 in water and k_L is the gas-liquid mass transfer coefficient calculated as in equation (6.13).

If x the spatial coordinate representing the distance from the gas-liquid interface, the equations of mass balance of reactant and product in the liquid film will be:

$$0 < x < \delta$$

$$\frac{\partial C_{CO_{2(l)}}}{\partial t} = D_{CO_2} \frac{\partial^2 C_{CO_{2(l)}}}{\partial x^2} - \dot{r_1} - \dot{r_4} \tag{6.51}$$

$$\frac{\partial C_{OH^-}}{\partial t} = D_{OH^-} \frac{\partial^2 C_{OH^-}}{\partial x^2} - \dot{r_1} - \dot{r_2} - \dot{r_3} \tag{6.52}$$

$$\frac{\partial C_{H^+}}{\partial t} = D_{H^+} \frac{\partial^2 C_{H^+}}{\partial x^2} - \dot{r_3} + \dot{r_4} \tag{6.53}$$

$$\frac{\partial C_{HCO_3^-}}{\partial t} = D_{HCO_3^-} \frac{\partial^2 C_{HCO_3^-}}{\partial x^2} \dot{r_1} - \dot{r_2} + \dot{r_4} \tag{6.54}$$

$$\frac{\partial C_{CO_3^{2-}}}{\partial t} = D_{CO_3^{2-}} \frac{\partial^2 C_{CO_3^{2-}}}{\partial x^2} + \dot{r_2} - \dot{r}_{MgCO_3} \tag{6.55}$$

$$\frac{\partial C_{Mg^{2+}}}{\partial t} = D_{Mg^{2+}} \frac{\partial^2 C_{Mg^{2+}}}{\partial x^2} - \dot{r}_{MgCO_3} \tag{6.56}$$

Where the reaction rates $\dot{r_j}$ and the crystallization rate $\dot{r}_{MgCO_3}$ are defined like in the previous section.

With this assumption the concentration of the species and the reaction rates (which are in turn functions of the concentrations) will depend both on the time and on a space coordinate x representing the distance from the gas-liquid interface.

Neglecting the diffusional transport for the precipitated particles through the liquid film and assuming a size independent growth rate, the number population balance and the moments of the distribution can be expressed as in Hotomsky and Jones (1995):

$$\frac{\partial n(x,t,L)}{\partial t} + G \frac{\partial n(x,t,L)}{\partial L} = 0 \tag{6.57}$$

$$\frac{\partial m_j(x,t)}{\partial t} = jG(x,t)m_{j-1}(x,t) + B(x,t)L_0^j \qquad (6.58)$$

Where B and G are defined like in the previous paragraph but here the supersaturation $S(x,t)$ is a function both of the time and of the spatial coordinate.

Since the process is described by a system of partial derivative equations initial and boundary conditions must be defined.

At the initial time of the process the film is assumed to be well mixed and have the same composition of the bulk-liquid phase:

$For\ t = 0, and\ 0 < x < \delta$

$$C_{OH^-}(t=0,x) = \sqrt[3]{\frac{K_{SP(Mg(OH)_2)}}{4}} \qquad (6.59)$$

$$C_{Mg^{2+}}(t=0,x) = \frac{1}{2}C_{OH^-(t=0)} \qquad (6.60)$$

$$C_{H^+}(t=0,x) = \frac{10^{\left(pK_W + log\left(\frac{C_{OH^-}(t=0)}{1000}\right)\right)}}{1000} \qquad (6.61)$$

$$C_{CO_{2(l)}}(t=0,x) = 0 \qquad (6.62)$$

$$C_{HCO_3^-}(t=0,x) = 0 \qquad (6.63)$$

$$C_{CO_3^{2-}}(t=0,x) = 0 \qquad (6.64)$$

$$m_j(t=0,x) = 0 \qquad (6.65)$$

At the gas-liquid interface the following boundary conditions were implemented:

$For\ t > 0, and\ x = 0$

$$C_{CO_{2(l)}}(x = 0) = C_{CO_{2(l)}(i)} = p_{CO_2}H \tag{6.66}$$

$$\frac{\partial C_{OH^-}}{\partial x}(t, x = 0) = \frac{\partial C_{H^+}}{\partial x}(t, x = 0) = \frac{\partial C_{HCO_3^-}}{\partial x}(t, x = 0) = \frac{\partial C_{CO_3^{2-}}}{\partial x}(t, x = 0) = \frac{\partial C_{Mg^{2+}}}{\partial x}(t, x = 0) = 0 \tag{6.67}$$

For $x = \delta$ boundary, which is representative of the bulk liquid phase, the mass balance for each reactant was implemented as in Wachi and Jones (1992):

$$t > 0, and\ x = \delta$$

$$\frac{\partial C_{CO_{2(l)}}}{\partial t} = -D_{CO_2} \cdot a_l \frac{\partial C_{CO_{2(l)}}}{\partial x} - \dot{r_1} - \dot{r_4} \tag{6.68}$$

$$\frac{\partial C_{OH^-}}{\partial t} = -D_{OH^-} \cdot a_l \frac{\partial C_{CO_{2(l)}}}{\partial x} - \dot{r_1} - \dot{r_2} - \dot{r_3} + a_s N_{OH^-} \tag{6.69}$$

$$\frac{\partial C_{H^+}}{\partial t} = -D_{H^+} a_l \frac{\partial C_{H^+}}{\partial x} - \dot{r_3} + \dot{r_4} \tag{6.70}$$

$$\frac{\partial C_{HCO_3^-}}{\partial t} = -D_{HCO_3^-} a_l \frac{\partial C_{HCO_3^-}}{\partial x} - \dot{r_1} - \dot{r_2} + \dot{r_4} \tag{6.71}$$

$$\frac{\partial C_{CO_3^{2-}}}{\partial t} = -D_{CO_3^{2-}} a_l \frac{\partial C_{HCO_3^-}}{\partial x} + \dot{r_2} - \dot{r}_{MgCO_3} \tag{6.72}$$

$$\frac{\partial C_{Mg^{2+}}}{\partial t} = -D_{Mg^{2+}} a_l \frac{\partial C_{Mg^{2+}}}{\partial x} - \dot{r}_{MgCO_3} + a_s N_{Mg^{2+}} \quad (6.73)$$

Where a_l is the surface specific area for the gas-liquid mass transfer defined as in equation (5.9).

We assume here that the dissolving particles of magnesium hydroxide do not penetrate the liquid film surrounding the gas bubbles but are contained in the bulk liquid phase, so $a_s N_{OH^-}$ and $a_s N_{Mg^{2+}}$, which are respectively the rate of OH^- and Mg^{2+} ions generation due to the dissolution of $Mg(OH)_2$ particles, were considered only at the $x = \delta$ boundary.

The boundary condition in the bulk phase set for each reactant was then:

$$C_i(x = \delta) = C_{i(b)}$$

Where $C_{i(b)}$ is the concentration of the reactant i in the bulk liquid phase.

5.2.2.2 DIFFUSING CRYSTALS IN THE FILM MODEL

If also a diffusional transport of the precipitated particles through the liquid film is kept in account, the population balance describing the system will be expressed as:

$$\frac{\partial n(x,t,L)}{\partial t} + G\frac{\partial n(x,t,L)}{\partial L} = D_P\frac{\partial^2 n(x,t,L)}{\partial x^2} \tag{6.74}$$

Where D_P is the diffusional coefficient of the precipitated particles.
Following the procedure adopted by Rigopoulos and Jones (2001) the moment transformation of the population balance and the diffusion coefficient of particles were expressed as follow:

$$D_P = \frac{k_B T}{3\pi\mu L} \tag{6.75}$$

$$\frac{\partial m_j(x,t)}{\partial t} = jG(x,t)m_{j-1}(x,t) + B(x,t)L_0^j + D_P\frac{\partial^2 m_j(x,t)}{\partial x^2} \tag{6.76}$$

Where L represents the size of the crystal. To simplify the calculation L in equation (6.75) was calculated as a time and space dependent volume-based average size defined as:

$$L(x,t) = \frac{m_3(x,t)}{m_2(x,t)} \tag{6.77}$$

Since, in this case, the moments of the crystal size distribution are not only function of the local concentrations as in the previous model, boundary conditions must be implemented in equation (6.76):

$For\ t > 0, and\ x = 0$

$$\frac{\partial m_j}{\partial x}(t, x = 0) = 0 \tag{6.78}$$

For $t > 0, and\ x = \delta$

$$\frac{\partial m_j(\delta,t)}{\partial t} = jG(x = \delta, t)m_{j-1}(x = \delta, t) + B(x = \delta, t)L_0^j - D_P a_l \frac{\partial m_j}{\partial x}(t, x = \delta) \tag{6.79}$$

Initial conditions for the moments m_j and mass balances, initial and boundary conditions for the ionic species were defined as in the previous model.

6 IMPLEMENTATION AND RESULTS

Since the system is quite complicated and requires the simultaneous solution of many differential equations, numerical methods were adopted to run simulations of the three models described.

The systems of ODE and PDE for the numerical solution of the clear film and 'crystal in the film models respectively were implemented in MATLAB.

In the case of the crystal in the film models the length of the stagnant film was discretized in 10 intervals of the same length. The method of lines was used to solve the resulting system of PDE adopting a central finite difference scheme for the spatial coordinate x.

After implementing the two mathematical models on MATLAB, the operational conditions used by Han et al. (2014) were set to compare the experimental results with the values calculated numerically.

6.1 $MgCO_3$ PRECIPITATION

The operational conditions and the characteristics of the experimental setup used by Han et al. (2014) are summarized in Table 1.

TABLE 1: Operational conditions for $MgCO_3$ precipitation by Han et al (2014).

Symbol	Parameter	Unit	Value
T	Temperature	$°C$	25
P	Pressure	atm	1
V	Volume of liquid	m^3	0.0025
p_{CO_2}	CO_2 Partial pressure	atm	1
$m_{Mg(OH)_2}$	Mass of $Mg(OH)_2$	kg	0,1
d_P	Initial $Mg(OH)_2$mean particles diameter	μm	4.6

N_P	Power number for Rushton turbine	-	5.5
α	Constant for Ruston turbine	-	0.783
β	Constant for Ruston turbine	-	0.459
H	Impeller' height	m	0.054
T	Impeller's diameter	m	0.01
N	Stirring rate	rpm	560
Q	Gas flow rate	l/min	1

At these operational conditions the values calculated for the gas-liquid mass transfer coefficient the specific interfacial area and the length of the film were:

TABLE 2: Calculated mass-transfer parameters for $MgCO_3$ precipitation

k_L	m/s	0.001328
a_l	m^{-1}	12.5
δ	m	$1.45 \cdot 10^{-6}$

The values of the physic-chemical parameter implemented in the model are summarized in Table 3.

TABLE 3 Physical-chemical parameters for $MgCO_3$ precipitation

H	$mol/(m^3 \cdot atm)$	35	Harned et al.(1943)
k_{11}	$m^3/(mol \cdot s)$	8.4	Plummer et al.(1982)
k_{12}	s^{-1}	$2 \cdot 10^{-4}$	
k_{21}	$m^3/(mol \cdot s)$	$6 \cdot 10^{6}$	
k_{22}	s^{-1}	$1.2 \cdot 10^{6}$	
k_{31}	$m^3/(mol \cdot s)$	$1.4 \cdot 10^{8}$	
k_{32}	$mol/(m^3 \cdot s)$	1,3	
k_{41}	s^{-1}	$2.4 \cdot 10^{-2}$	
k_{42}	$m^3/(mol \cdot s)$	57	
$K_{SP(Mg(OH)_2}$	mol^3/m^9	$5.61 \cdot 10^{-3}$	Booster et al.(2002)
K_{spMgCO_3}	mol^2/m^6	0.0682	Hu and Deng (2004)
D_{CO_2}	m^2/s	$1.92 \cdot 10^{-9}$	Frank, Kuipers(1996)
D_{OH^-}	m^2/s	$5.27 \cdot 10^{-9}$	
D_{H^+}	m^2/s	$9.31 \cdot 10^{-9}$	
$D_{HCO_3^-}$	m^2/s	$1.19 \cdot 10^{-9}$	
$D_{CO_3^{2-}}$	m^2/s	$0.923 \cdot 10^{-9}$	
$D_{Mg^{2+}}$	m^2/s	$0.706 \cdot 10^{-9}$	Yuan-Huy and Gregory (1973)
k_n	$mol^{-n}m^{3n-3}/s$	$1.406 \cdot 10^{7}$	Fitted parameters
k_g	$mol^{-g}m^{3g+1}/s$	$1.364 \cdot 10^{-12}$	
n	-	3.205	
g	-	1.598	

Experimental data were available for the time evolution of the values of pH, mass of $Mg(OH)_2$, concentration of Mg^{2+} in the liquid phase and mass of precipitated $MgCO_3$.

6.1.1 RESULTS OF THE CLEAR FILM MODEL

Kinetic parameters for nucleation and crystal growth were not available in the literature thus the values implemented in the model were fitted on the experimental data using the function 'fminsearch' of MATLAB. This function has been used to identify the minima of the difference between the experimental data and the predictions of the clear film model.

Figures 6, 7, 8, 9 show the results obtained using the clear film model after having fitted the parameters, compared with experimental data.

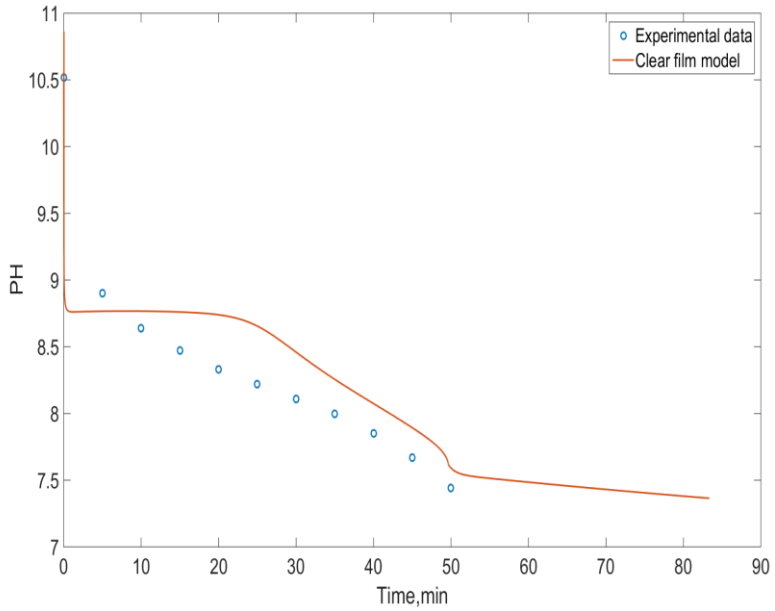

FIGURE 5: Comparison of pH trend with experimental data in $MgCO_3$ precipitation in the clear film model

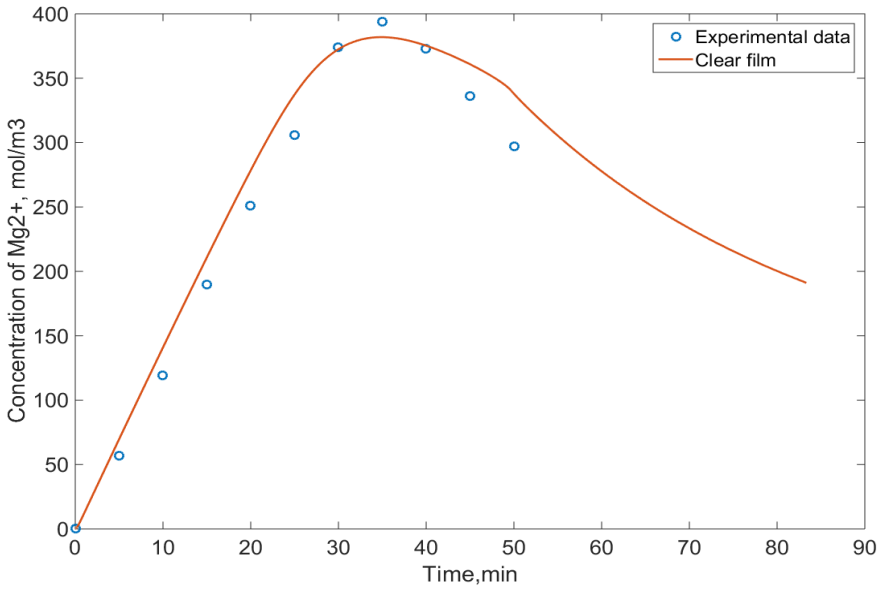

FIGURE 6: Comparison of Mg^{2+} concentration with experimental data in $MgCO_3$ precipitation in the clear film model

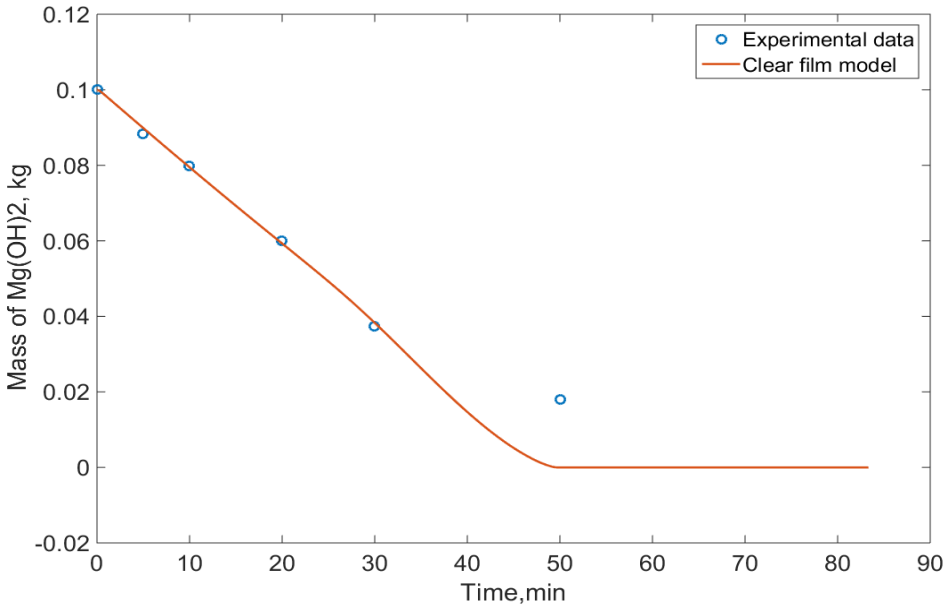

FIGURE 7: Comparison of mass of dissolving $Mg(OH)_2$ with experimental data in $MgCO_3$ precipitation in the clear film model

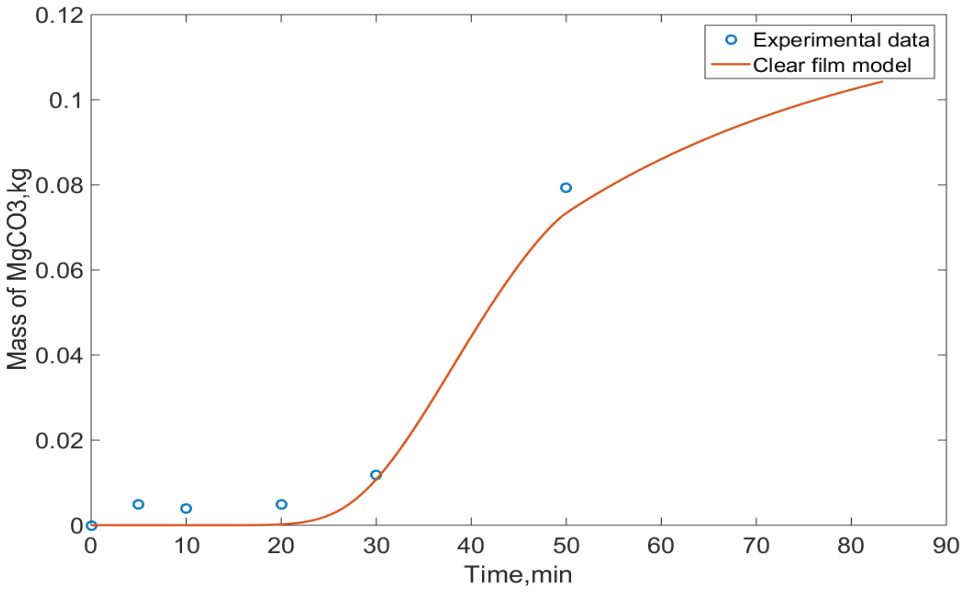

FIGURE 8: Comparison of mass of precipitated $MgCO_3$ with experimental data in $MgCO_3$ precipitation in the clear film model

Quite good agreement between experimental results and the model implemented were obtained under these operating conditions.

Both experimental data and the model show a sudden drop in the value of the pH at the beginning of the process that indicates that the depletion of OH^- by the reactions r_1 and r_2 cannot be balanced by the intake due to the dissolution of the $Mg(OH)_2$ particles.

The drop of the concentration of OH^- in the liquid phase enhances the dissolution rate of Magnesium hydroxide which dissolves gradually during the whole process (Fig.7).

The concentration in Mg^{2+} ions increase sharply due to the dissolution of $Mg(OH)_2$ while the pH in the solution drops since OH^- ions produced by the dissolution are depleted by reactions r_1 and r_2.

The increase of the Mg^{2+} concentration is not immediately accompanied by significant precipitation of solid $MgCO_3$.

In this initial phase of the process the liquid phase is supersaturated (Fig.9) thus the driving force for nucleation and growth rate of the crystals is positive. Nevertheless the depletion of Mg^{2+}due to precipitation is much lower than the Mg^{2+} production deriving from $Mg(OH)_2$ particles dissolution.

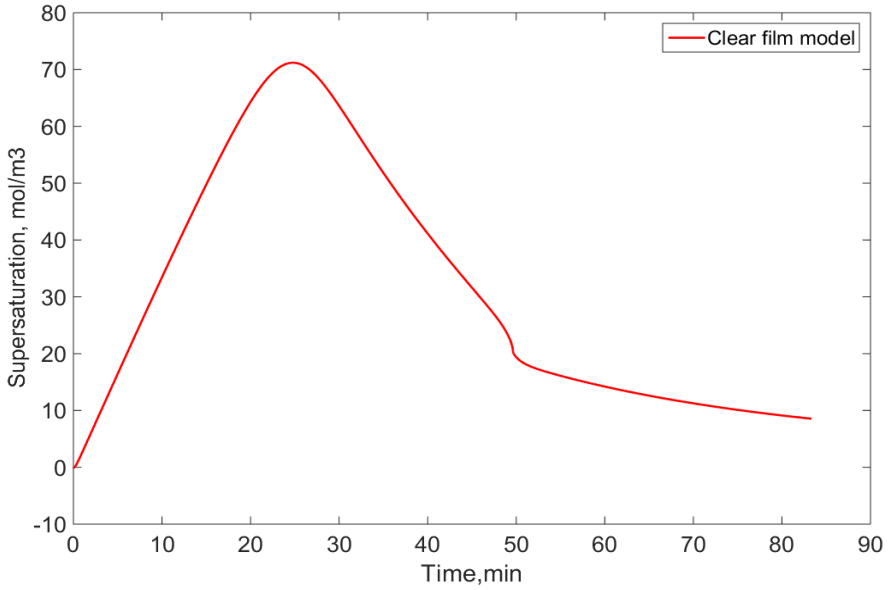

FIGURE 9: Time trend of supersaturation in $MgCO_3$ precipitation

6.1.2 COMPARISON OF THE MODELS

The same parameters obtained by the fitting procedure described were implemented in the "crystals in the film" model, at the same operating conditions. The comparison of the results obtained are shown in Fig 10 in which the time evolution of pH predicted by the clear film model are compared with the one predicted by the crystal film model for the $x = \delta$ boundary.

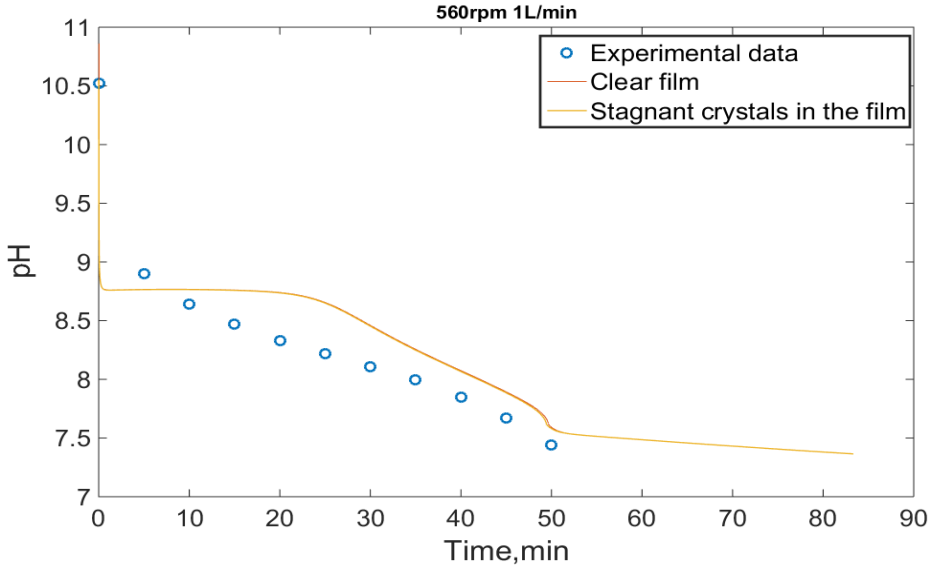

FIGURE 10: Comparison of the pH trend prediction by the two models in $MgCO_3$ precipitation

As can be seen from Figure 10, the two different models predicted approximately the same time trend of the pH in the process. Only by zooming on the figure it is possible to note that the diffusion of the ionic species in the gas-liquid film enhances the process, so that the drop of the pH predicted by the clear film model is slightly delayed compared to the 'crystals in the film model'.

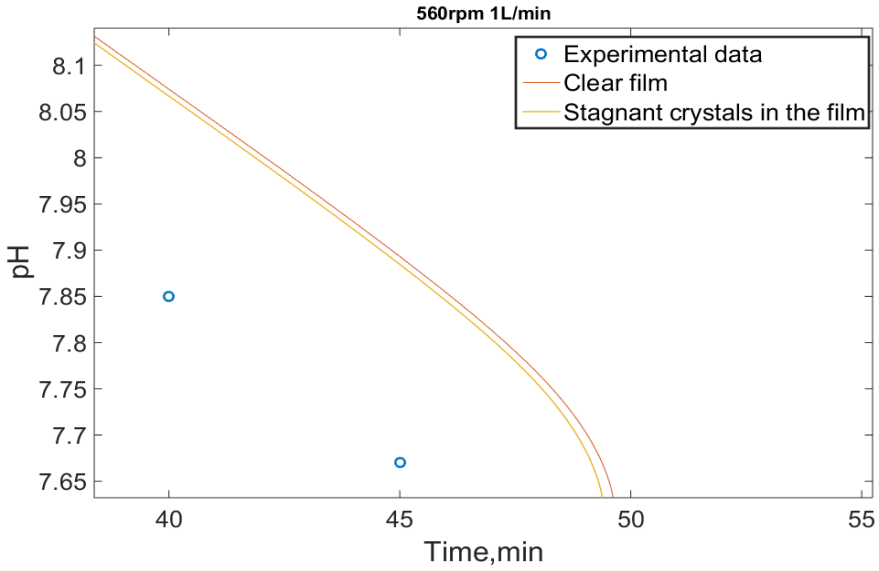

FIGURE 11: Detail of the difference between the models in $MgCO_3$ precipitation

The same delay of the clear film model compared to the "crystals in the film" model, can be observed in the prediction of the increase in Mg^{2+} concentration, and the mass of dissolving $Mg(OH)_2$.

This very small time difference in the predictions by the two models shows that the extent of reactions and precipitation occurring in the gas-liquid film is negligible. CO_2 absorbed at the gas liquid interface diffuse fast to the bulk due to the thin length of the gas liquid film while the reactions occurring in the film are slow.

As can be seen from Table 1 reaction r_1 is not instantaneous kinetics while reaction r_2 is reversible and instantaneous and the participating species can be considered to be at equilibrium (Wachi and Jones, 1992). In these operational conditions, in which the gas-liquid interface concentration is high and the

stagnant liquid film surrounding the gas bubbles is thin, the diffusional transport of CO_2 across the film is fast while the kinetic of reaction $r_1$is not fast enough to enhance significantly the diffusion.

Only at the very initial phase of the process the whole amount of adsorbed CO_2 is depleted within the film (Figure 12).

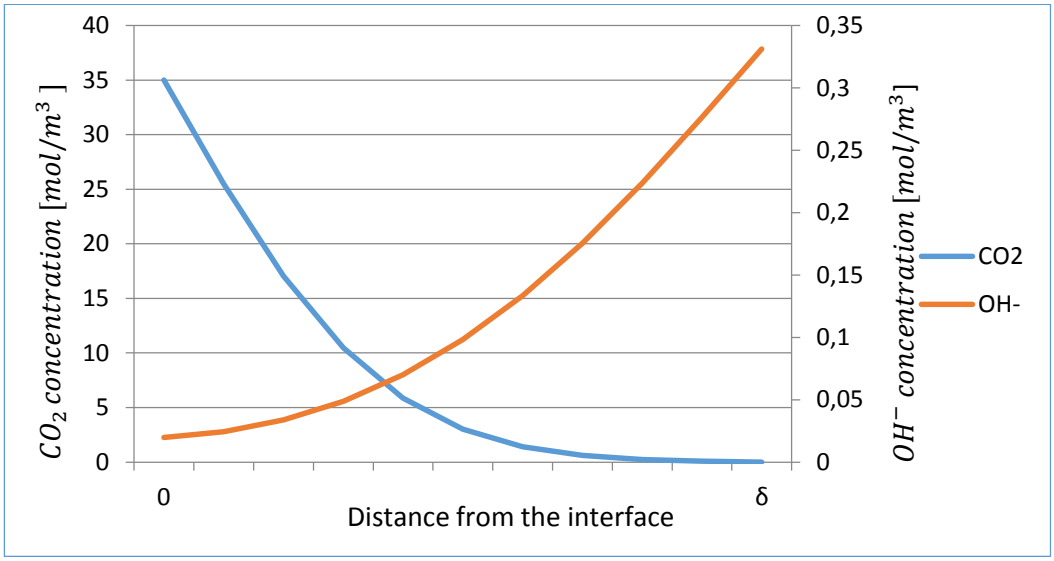

FIGURE 12: CO_2 and OH^- concentration profiles for t=0,1s in $MgCO_3$ precipitation

After a few seconds the concentration of OH^- in the system drops due to the slow kinetics of dissolution of the $Mg(OH)_2$ particles. As a consequence the kinetic of reaction r_1 will sharply slow down.

As the process proceeds the components diffuse through the film in short time due to the thin length of it but the kinetic of the reaction r_1 is not fast enough to induce a significant depletion of reactants.

In this situation the shape of the concentration profile of OH^- in the film is substantially flat and indicating that the diffusional transport of hydroxyl ions

from the bulk to the gas liquid interface is much faster than the rate of reaction r_1.

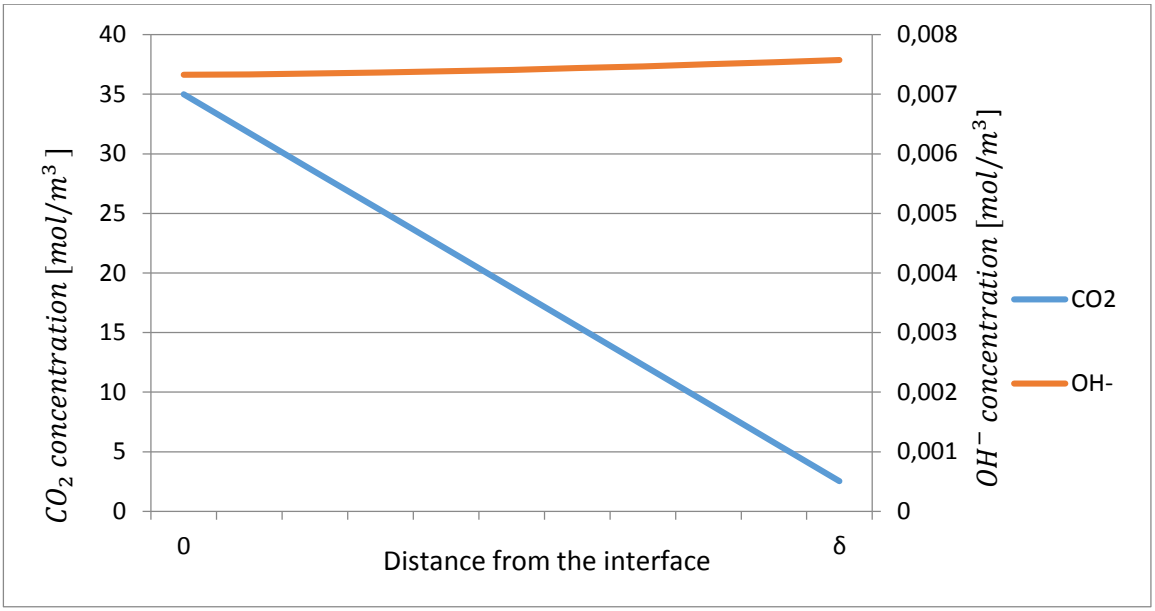

FIGURE 13: CO_2 and OH^- concentration profiles for t=10s in $MgCO_3$ precipitation

The profile of carbon dioxide concentration has a linear shape indicating that the significance of CO_2. So the mass balance at the $x = \delta$ boundary can be approximated as:

$$\frac{\partial C_{CO_{2(l)}}(x=\delta)}{\partial t} = -D_{CO_2} \cdot a_l \frac{\partial C_{CO_{2(l)}}}{\partial x} - \dot{r_1} \approx D_{CO_2} \cdot a_l \left(\frac{C_{CO_{2(l)}(i)} - C_{CO_{2(l)(x=\delta)}}}{\delta} \right)$$

$$= k_l a_l (C_{CO_{2(l)}(i)} - C_{CO_{2(l)}})$$

As in the clear film model.

In this situation the concentrations of the reacting species are flat in the film meaning that the phenomena here are slow and have a low influence on the kinetic of the process.

FIGURE 14: CO_3^{2-} and Mg^+ concentration profiles for t=10s in $MgCO_3$ precipitation

Even when a high value of supersaturation is reached after about 30 minutes from the beginning of the process, the concentrations of reactive ions are homogeneous across the film meaning that the diffusional transport of Mg^{2+} from the bulk is faster than its depletion due to $MgCO_3$ precipitation.

The rate of precipitation in the film is the same as in the bulk and thus can be neglected since the volume of the liquid film can be considered negligible compared to the volume of the bulk.

FIGURE 15: CO_3^{2-} and Mg^+ concentration profiles for t=30 min in $MgCO_3$ precipitation

6.2 $CaCO_3$ PRECIPITATION FROM A $Ca(OH)_2$ SLURRY

The same experiment was repeated by Han et al.(2014) using the same experimental setup but bubbling CO_2 into a suspension of $Ca(OH)_2$ particles for $CaCO_3$ precipitation.

Two different operational conditions were adopted as reported in Table 4.

TABLE 4: Operational conditions for $CaCO_3$ precipitation by Han et al (2014).

	N (Stirring rate) [rpm]	p_{CO_2} (CO_2 Partial pressure)	Q(Gas flow rate) [l/min]
Experiment 1	650	1	1
Experiment 2	650	1	5

At these operational conditions the values calculated for the gas-liquid mass transfer coefficient and the specific interfacial are reported in Table 5.

TABLE 5: Calculated mass-transfer parameters for $CaCO_3$ precipitation

	$k_L[m/s]$	$a_l[m^{-1}]$
Experiment 1	0.00149	16.0
Experiment 2	0.00137	38.87

While the lengths of the gas-liquid film calculated for each one of the two experiments were:

TABLE 6: Calculated lengths of gas-liquid film for $CaCO_3$ precipitation

	δ $[\mu m]$
Experiment 1	1.28
Experiment 2	1.40

Unlike the case of $MgCO_3$, kinetics parameters for nucleation and growth of $CaCO_3$ are available in the literature. The values implemented in the model are reported in Table 7.

TABLE 7: Physical-chemical parameters for $CaCO_3$ precipitation from a $Ca(OH)_2$ slurry.

$K_{SP(Ca(OH)_2}$	mol^3/m^9	$5.5{\cdot}10^3$	Jones et al,1992
K_{spCaCO_3}	mol^2/m^6	0.00347	Jones et al,1992
$D_{Ca^{2+}}$	m^2/s	$0.792 \cdot 10^{-9}$	Yuan-Huy and Gregory (1973)
k_n	$mol^{-n}m^{3n-3}/s$	$1 \cdot 10^7$	Jones et al,1992
k_g	$mol^{-g}m^{3g+1}/s$	$8.06 \cdot 10^{-9}$	
n	-	4.2	Jones et al,1992
g	-	2	

The time evolution of the pH obtained by the implementation of the models at the same operating conditions is reported in Figures 16 and 17.

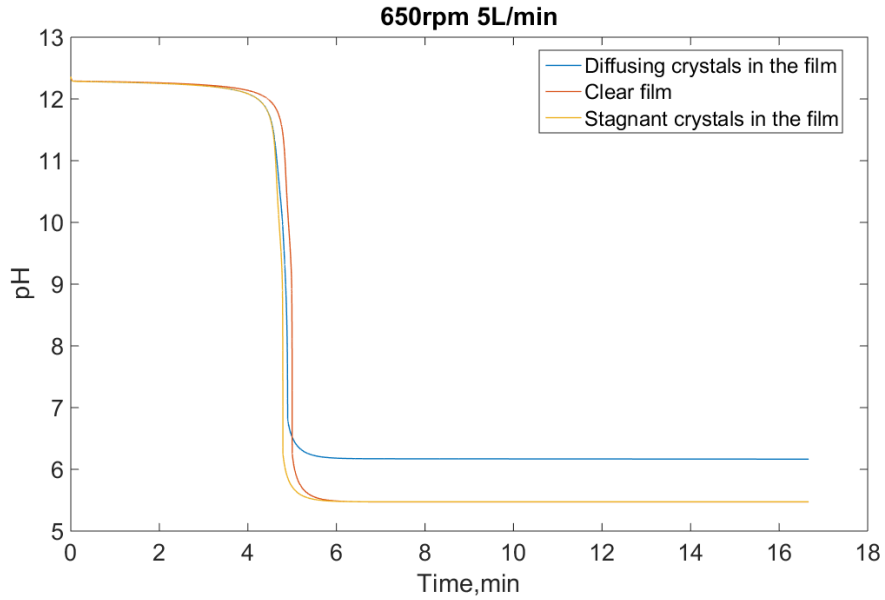

FIGURE 16: Comparison of the pH trend prediction by the three models in $CaCO_3$ precipitation with a gas flow rate of 5 L/min

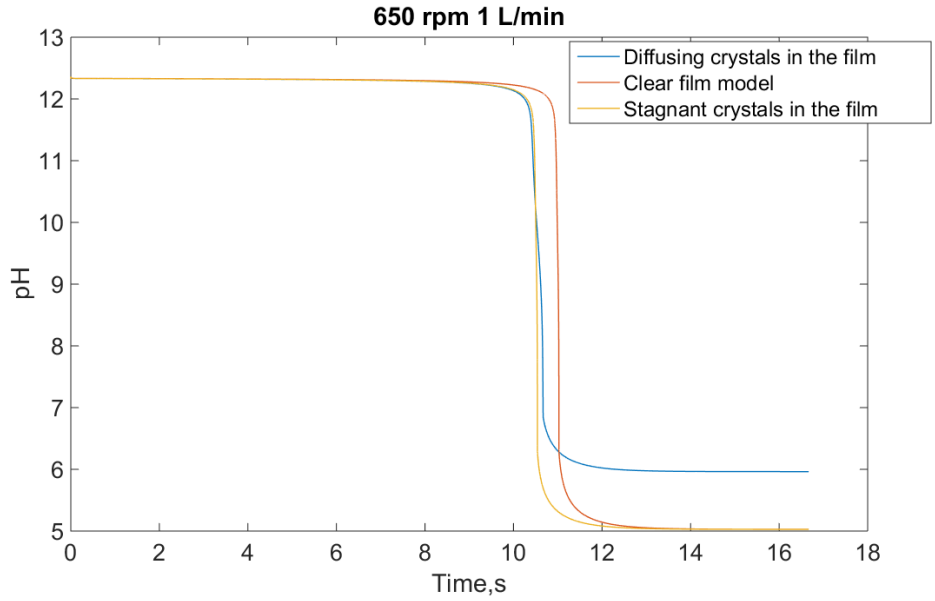

FIGURE 17: Comparison of the pH trend prediction by the three models in $CaCO_3$ precipitation with a gas flow rate of 1 L/min

The models were able to predict the trend in the pH drop experimentally observed by Han et al. (2014) and the enhancement that an increasing gas flow rate has on the $CaCO_3$ precipitation.

Nevertheless, in both the operational conditions the predicted evolution of the process was faster than the one measured experimentally.

The time delay in the prediction of the drop of the pH by the clear film model is more remarkable in this case compared to the previous case of $MgCO_3$ precipitation. This happen because in the first phase of the process the concentration of hydroxyl ion in the system is high. Consequently the rate of reaction between absorbed CO_2 and OH^- within the gas-liquid film, neglected by the clear film model, will be faster having an enhancing effect on the gas absorption and on the precipitating process in general.

In both of the cases the model in which the diffusion of the particles is taken in account predicted a final value of the pH was different from the one predicted by the two others. Checking the mass balance in the system after the numerical simulation some problems were found. The implementation of this model, in this case, would require further analysis.

As can be observed by Figures 18 and 19, time of dissolution and precipitation predicted by the models were much shorter if compared to the previous case of $MgCO_3$ precipitation confirming the experimental observation by Han et al. (2014). In Figure 18 the two models taking into account reactions and precipitation in the film predicted the same kinetics of dissolution of the $Ca(OH)_2$ particles.

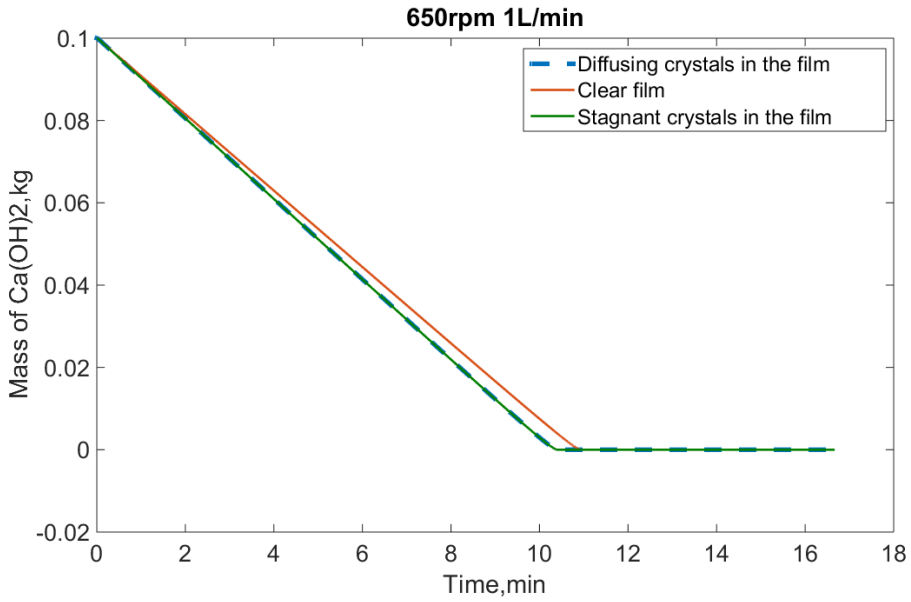

FIGURE 18: Comparison of the mass of dissolving $Ca(OH)_2$ prediction by the three models in $CaCO_3$ precipitation with a gas flow rate of 1 L/min

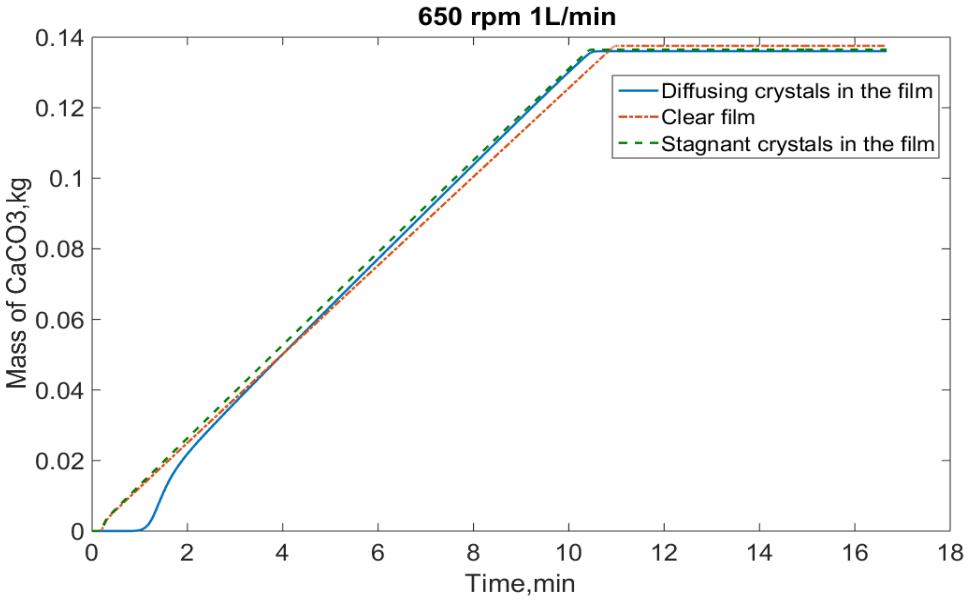

FIGURE 19: Comparison of the mass of precipitating $CaCO_3$ prediction by the three models in $CaCO_3$ precipitation with a gas flow rate of 1 L/min

The time evolution predicted by the models for the concentration of Ca^{2+} and CO_3^{2-} are reported in the Figures 20 and 21: after a peak in the concentration of reactive ions is reached, the precipitation process occurs at a constant rate. During this precipitation period the concentration of both Ca^{2+} and CO_3^{2-} since the rate of $CaCO_3$ is equaled by the rate of CO_3^{2-} absorption and $Ca(OH)_2$. dissolution.

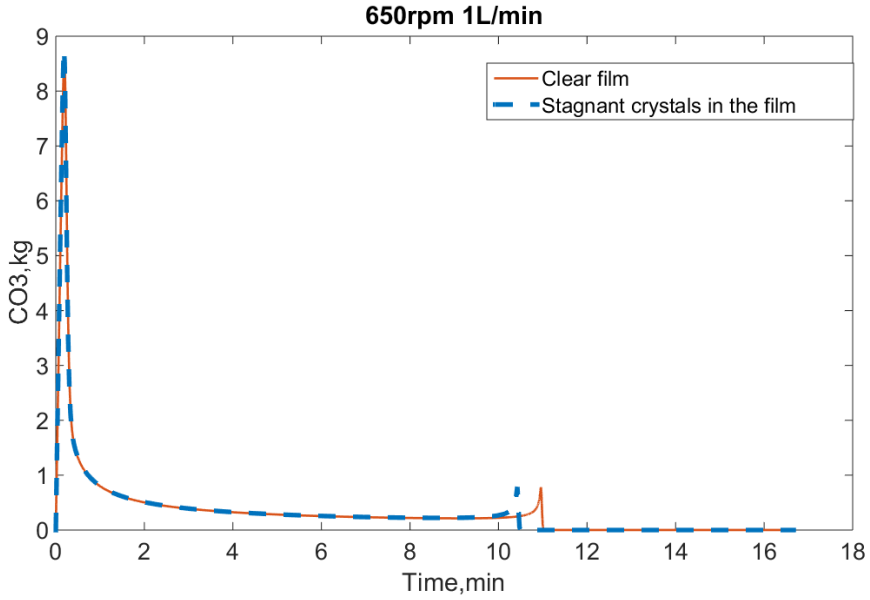

FIGURE 20: Comparison of the CO_3^{2-} trend prediction by the two models in $CaCO_3$ precipitation with a gas flow rate of 1 L/min

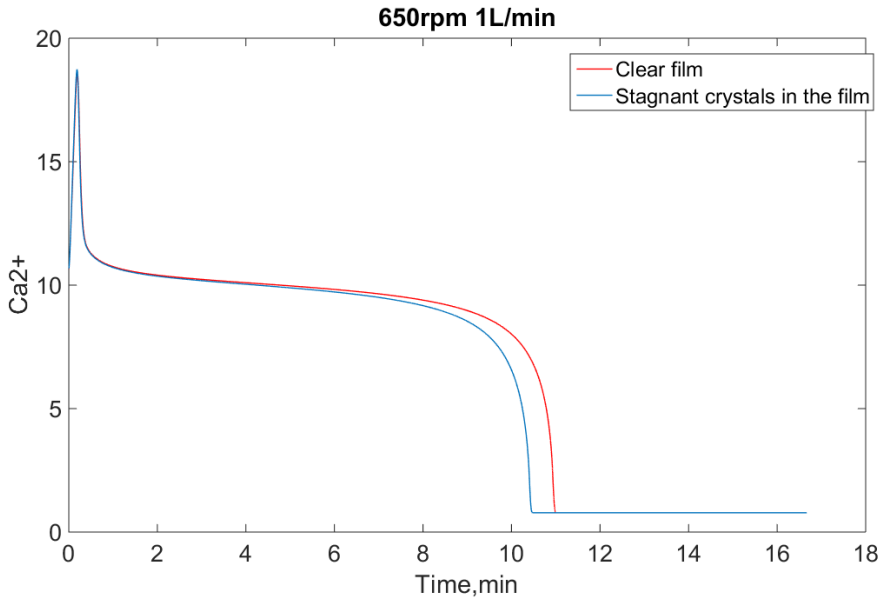

FIGURE 21: Comparison of the Ca^{2+} trend prediction by the two models in $CaCO_3$ precipitation with a gas flow rate of 1 L/min

Approaching the end of dissolution the concentration of Ca^{2+} decrease sharply reaching a final value of approximately 0.78 mol/m^3.

As the concentration of Ca^{2+} drops, the precipitation rate slows down and the concentration of CO_3^{2-} will initially increase (Fig20). After this initial growth CO_3^{2-} disappear from the system being converted into HCO_3^- since the equilibrium of reaction r_2 shifts to the left as the pH in the system drops.

Figures 22 and 23 report the concentration profiles obtained through the liquid film in the crystal film model during the first phase of the process in which the pH is stable at ≈12.3.

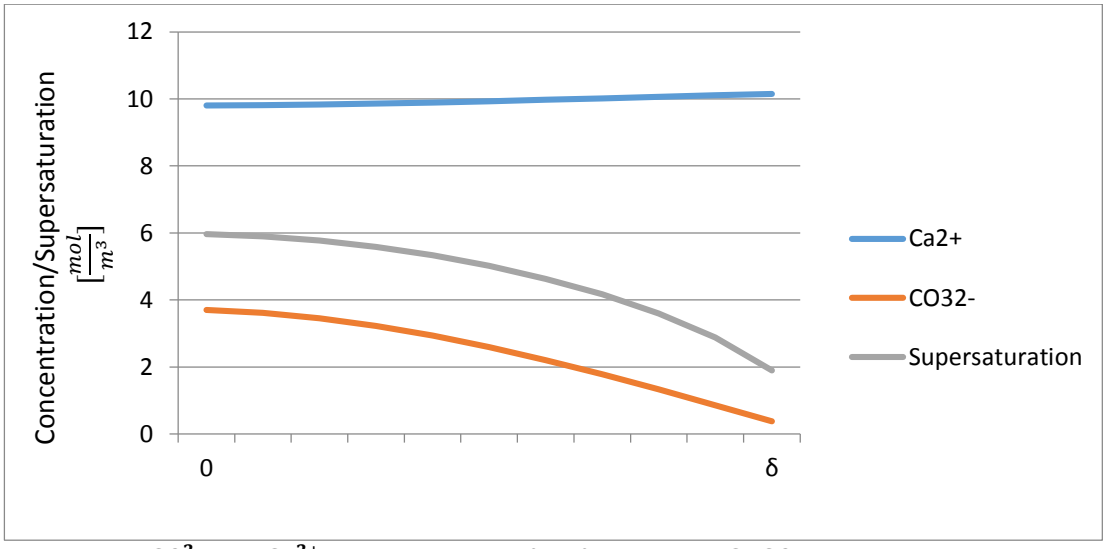

FIGURE 22: CO_3^{2-} and Ca^{2+} concentration profiles for t=100s in $CaCO_3$ precipitation with a gas flow rate of 1 L/min

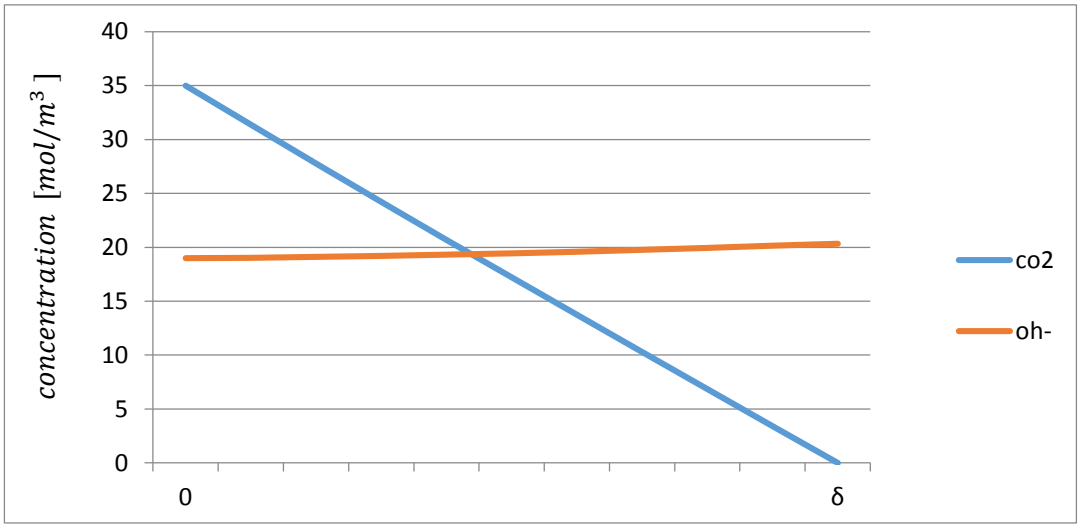

FIGURE 23: CO_2 and OH^- concentration profiles for t=100s in $CaCO_3$ precipitation precipitation with a gas flow rate of 1 L/min

We can see that in this case the concentration of OH^- is high in the film. In this situation the reaction between hydroxyl ion and absorbed CO_2 will be fast, enhancing the gas absorption if compared to the crystal film model in which reactions occur in the bulk only.

CO_3^{2-} concentration is maximum at the interface where the rate of reaction between CO_2 and OH^- is highest. A significant amount of carbonate is depleted in the film and the supersaturation is lower in the bulk meaning that the crystallization is occurring faster in the film. Concentration of Ca^{2+} is almost constant in the film, this means that the diffusional transport of calcium from the bulk is faster than its depletion due to $CaCO_3$ precipitation.

6.2.1 $CaCO_3$ PRECIPITATION FROM $Ca(OH)_2$ SLURRY USING DILUTED CO_2

The models were also tested assuming to feed in the reactor a mixture of CO_2 and an inert gas.

Figure 24 shows the result obtained for a total gas flow rate of 1l/min in which the molar fraction of CO_2 was assumed to be 0.25.

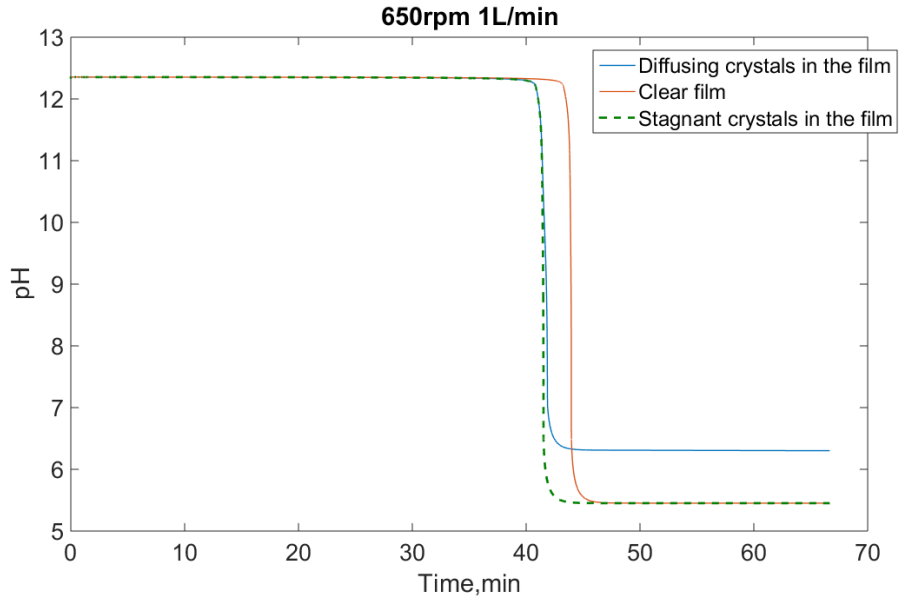

FIGURE 24: Comparison of the pH trend prediction by the models in $CaCO_3$ precipitation with a gas flow rate of 1 L/min and a molar fraction of CO_2 in the inlet gas $y_{CO_2} = 0.25$.

As we can see from the figure, the whole process was slower due to the low concentration of CO_2 in the gas. The difference between the two models in terms of prediction of the time evolution of the process is bigger than in the previous case but approximately grew up proportionally to the growth in the time duration of the whole process. This could mean that, in the case in which the liquid film is very thin, the concentration of CO_2 in the gas phase has low influence on the extent of the phenomena of reaction and precipitation occurring in the film.

6.3 $CaCO_3$ PRECIPITATION FROM A $Ca(OH)_2$ SOLUTION IN A GAS-LIQUID FLAT INTERFACE REACTOR

The three models for reactive of gas liquid mass transfer with reactive precipitation were also tested in another operating condition described in Wachi and Jones (1991b).

In this work batch precipitation of calcium carbonate by carbonation of lime water was operated in a batch flat-interface gas-liquid agitated vessel at different stirring rates. The gas fed to the reactor was not pure CO_2 as in the previous experimental conditions but a mixture of carbon dioxide and an inert gas. The molar fraction of CO_2 was 0.25.

The values reported by the authors for the gas-liquid mass transfer coefficient, the specific surface area and the length of the stagnant film at the gas-liquid interface at different operational conditions are reported in Table 8.

TABLE 8: Operational conditions and mass transfer parameters from Wachi and Jones (1991b)

Stirring rate [rpm]	k_l $[\frac{m}{s}]$	δ [m]	$Ca(OH)_2$ Concentration $[\frac{mol}{m^3}]$	Molar fraction of CO_2 in the inlet gas
200	$1.96 \cdot 10^{-5}$	$7.8 \cdot 10^{-5}$	5.2	0.25
350	$2.91 \cdot 10^{-5}$	$5.2 \cdot 10^{-5}$	5.2	0.25

The figure shows that in this case the difference in the predictions of the time evolution of the process obtained by the models is significant.

The clear film model in this case predicts a much slower evolution of the process which is far from the real behavior of the process experimentally observed by Wachi and Jones(1991b).

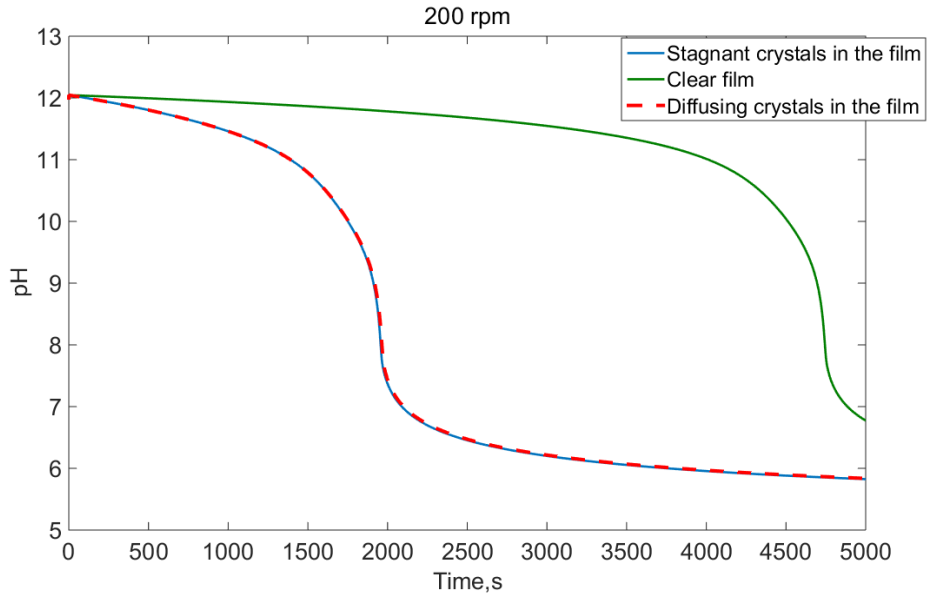

FIGURE 25: Comparison of the pH trend prediction by the models in $CaCO_3$ precipitation from a $Ca(OH)_2$ solution with a molar fraction of CO_2 in the inlet gas $y_{CO_2} = 0.25$ and a stirring rate of 200rpm.

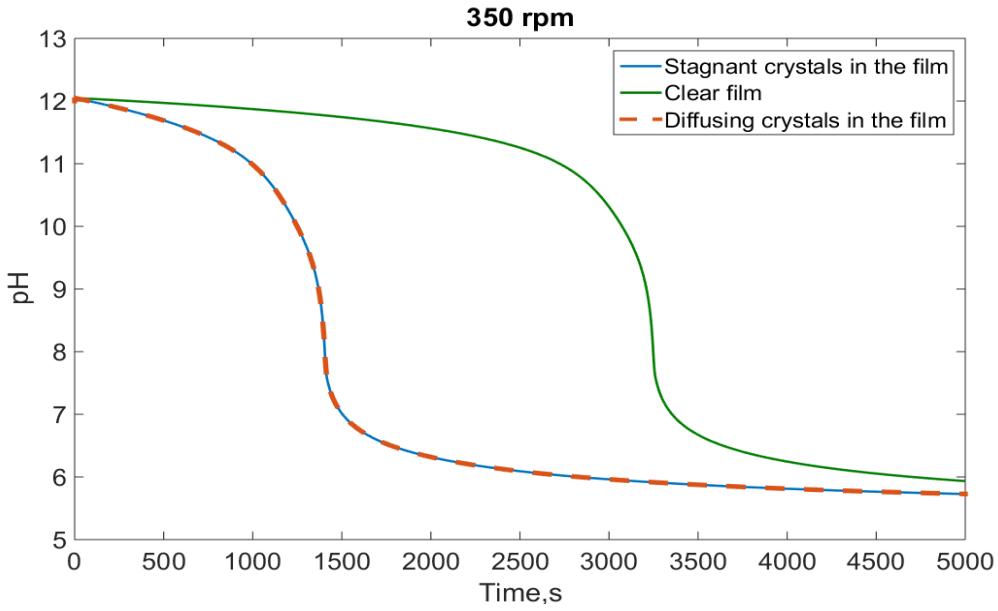

FIGURE 26: Comparison of the pH trend prediction by the models in $CaCO_3$ precipitation from a $Ca(OH)_2$ solution with a molar fraction of CO_2 in the inlet gas $y_{CO_2} = 0.25$ and a stirring rate of 350rpm.

This happened because, in these experimental conditions, in which the gas-liquid film is thick and the concentration of CO_2 in the inlet gas is low, neglecting the reactions that occur in the film will lead to wide underestimation of the rate of gas-liquid mass-transfer.

The difference between the two models in which reaction and precipitation in the film are taken into account was found to be very small meaning that including a diffusive transport term for the precipitated particles within the film has a negligible influence on the prediction of the kinetics of the process.

Plotting for example the calculated profiles of concentration for a time t=100s we have the situation in Figure 27.

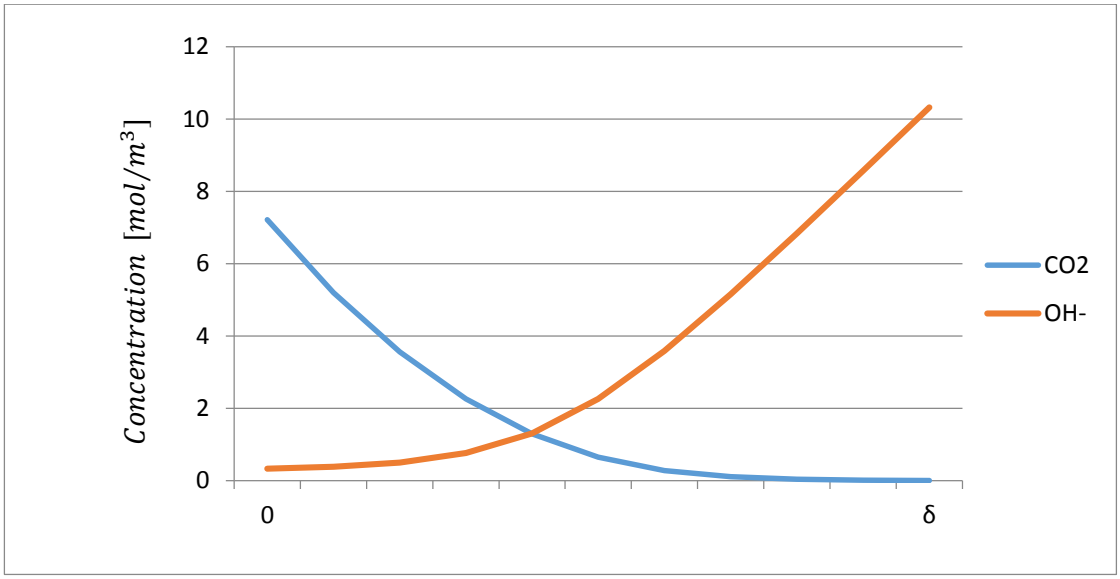

FIGURE 27: CO_2 and OH^- concentration profiles for t=100s in $CaCO_3$ precipitation from a $Ca(OH)_2$ solution with a molar fraction of CO_2 in the inlet gas $y_{CO_2} = 0.25$ and a stirring rate of 350 rpm.

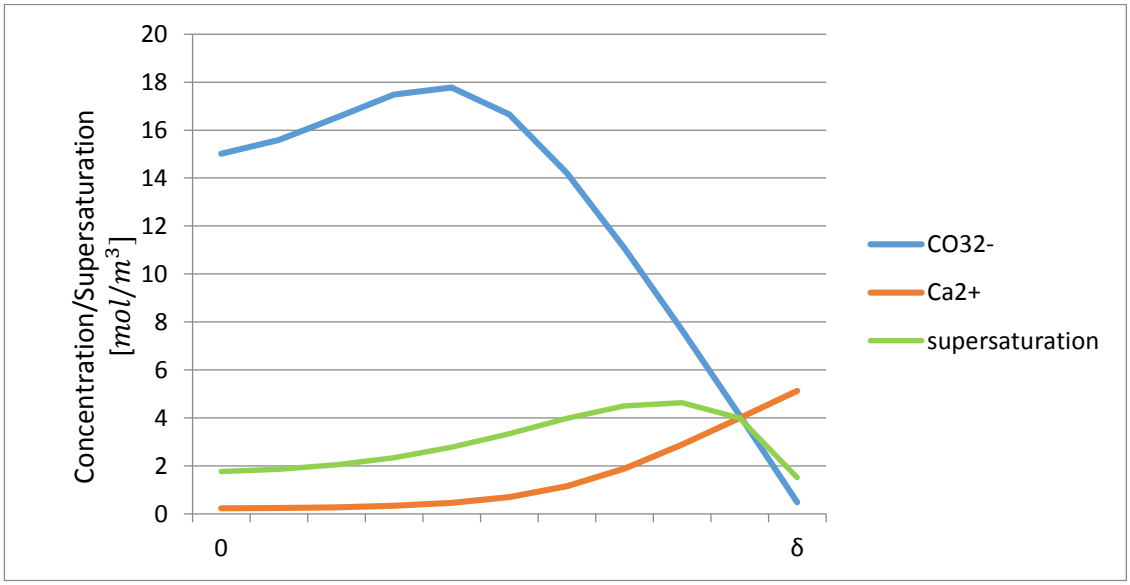

FIGURE 28: CO_3^{2-} and Ca^{2+} concentration profiles for t=100s in $CaCO_3$ precipitation precipitation from a $Ca(OH)_2$ solution with a molar fraction of CO_2 in the inlet gas $y_{CO_2} = 0.25$ and a stirring rate of 350 rpm.

As we can see from Figure 27 the amount of CO_2 absorbed is depleted within the film before reaching the bulk phase by diffusional transport. The reactions between CO_2 and OH^-generates high concentrations of carbonate ions that will precipitate reacting with calcium ions diffusing from the bulk liquid phase. We can see from Figure 28 that the highest values of supersaturation are reached in the film, meaning that the precipitation rate of $CaCO_3$ will be higher here than in the bulk. The entity of the phenomena occurring in the film has a strong influence on the kinetic of the process.

6.3.1 $CaCO_3$ precipitation from a $Ca(OH)_2$ solution in a gas-liquid flat interface REACTOR USING PURE CO_2

To investigate the influence of the CO_2 concentration in the feed gas on the performance of the models, the same experimental set up was simulated in the models but assuming to feed pure CO_2 in the flat-interface gas-liquid stirred vessel.

Figure 29 reports the time evolution of the pH in this other condition for a stirring rate of 200 rpm.

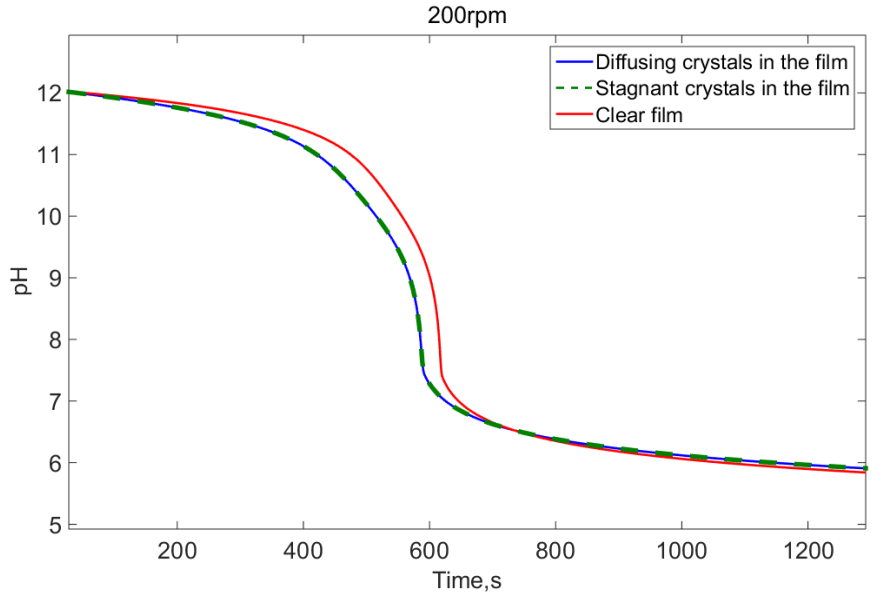

FIGURE 29: Comparison of the pH trend prediction by the models in $CaCO_3$ precipitation from a $Ca(OH)_2$ solution with a molar fraction of CO_2 in the inlet gas $y_{CO_2} = 1$.

Unlike the previous case, the difference between the results of the models were almost negligible. The two models keeping in account reaction and precipitation in the film predicted the same time trend of the process.

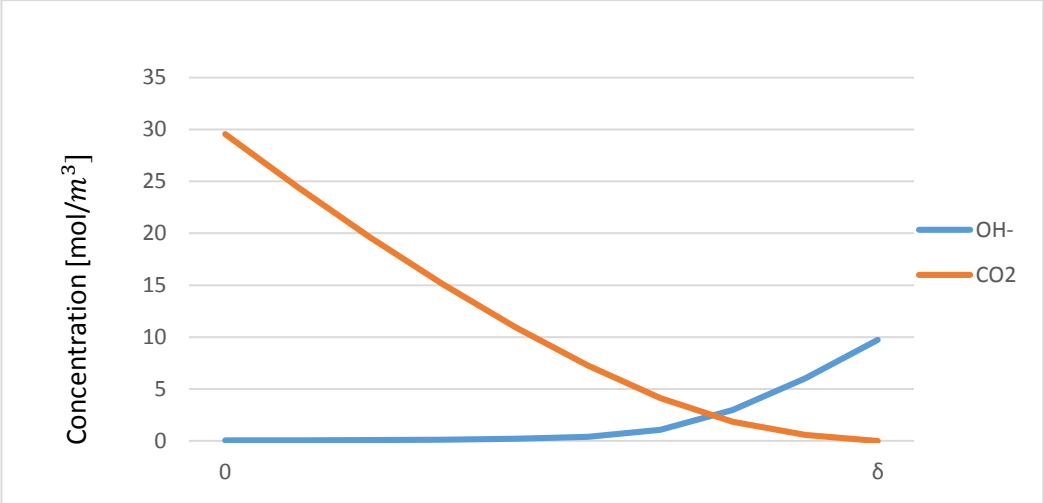

FIGURE 30 CO_2 and OH^- concentration profiles for t=100s in $CaCO_3$ precipitation from a $Ca(OH)_2$ solution with a molar fraction of CO_2 in the inlet gas $y_{CO_2} = 1$ and a stirring rate of 200 rpm.

In this case the reaction between CO_2 and OH^- will occur mostly in the part of the film closer to the bulk phase, while near the interface it will have a slow kinetic due to the low concentration of hydroxyl ions which are depleted by reaction r_1 before reaching the gas-liquid interface . The shifting of the 'reaction zone' towards the bulk phase can explain the small difference between the 'crystals in the film' model and the simplified model in which the reaction is assumed to occur in the bulk only.

7 CONCLUSIONS

Two different kind of models for reactive precipitation were developed implemented on MATLAB by coupling rate equations for particles dissolution, gas absorption and crystallization and, when possible, verified using experimental data.

In the first simplified model, the phenomena occurring in the gas-liquid film where neglected while in the second one the length of the film was discretized to solve numerically distributed mass balance equations for gas absorption with chemical reaction and distributed population balance. In this way it was possible to obtain concentrations profiles of the species in the gas-liquid film and quantify how the spatial non-uniformity of the supersaturation affects the precipitation rate.

The results reported show that the use of the simplified model is suitable depending on the operational conditions.

In all the simulation tested, neglecting the phenomena occurring in the film involved an under-estimation of the kinetics of the process but the extent of the difference between the predictions of the two models sometimes was negligible.

The parameters that affect the significance of the phenomena occurring in the film were found to be the concentration of CO_2 in the gas phase, the concentration of OH^- in the liquid phase, the length of the stagnant gas-liquid film and the precipitating rate.

In the first two simulated experiments the length of the film was low and the concentration of CO_2 was high so the diffusion time of the absorbed gas towards the bulk is short.

In the case of $MgCO_3$ precipitation, in which both the CO_3^{2-} production and depletion are slow due to a low concentration of OH^- and the slow kinetic of solid precipitation respectively, the rate of the reacting phenomena in the film was found to have small influence on the kinetics of the process.

In the case of $CaCO_3$ precipitation, instead, the reactions and precipitations in the gas-liquid film were found to have a quite higher rate in the gas-liquid film compared to the bulk phase.

Nevertheless only in some conditions this fact was significant on the kinetic of the whole process.

In the simulations in which pure CO_2 was supposed to be fed in the reactor the two models did not show very significant differences both in case of high mass-transfer resistance (flat interface reactor) and low mass transfer resistance (sparged reactor).

The only situation in which the phenomena occurring in the film were really significant was the combination of a low concentration of CO_2 in the gas phase and a high mass transfer resistance.

REFERENCES

Al-Rashed, M.H. & Jones, A.G. 1999, "CFD modelling of gas–liquid reactive precipitation", *Chemical Engineering Science,* vol. 54, no. 21, pp. 4779-4784.

Asai, S., Konishi, Y. & Kajiwara, T. 1989, "Effect of sparged gas on mass transfer between fine particles and liquids in an agitated vessel.", *Journal of Chemical Engineering of Japan,* vol. 22, no. 1, pp. 96-98.

Barret, P. & Bracconi, P. 2002, "Heterogeneous kinetics: from solid–gas reaction to solid–liquid dissolution", *Thermochimica acta,* vol. 388, no. 1, pp. 91-103.

Bharadwaj, H.K., Lee, J., Li, X., Liu, Z. & Keener, T.C. 2013, "Dissolution kinetics of magnesium hydroxide for CO 2 separation from coal-fired power plants", *Journal of hazardous materials,* vol. 250, pp. 292-297.

Bhavaraju, S., Russell, T. & Blanch, H. 1978, "The design of gas sparged devices for viscous liquid systems", *AIChE Journal,* vol. 24, no. 3, pp. 454-466.

Booster, J., Van Sandwijk, A. & Reuter, M. 2003, "Conversion of magnesium fluoride to magnesium hydroxide", *Minerals Engineering,* vol. 16, no. 3, pp. 273-281.

Chen, Y. & Wang, P. 1989, "Dissolution of spherical solid particles in a stagnant fluid: An analytical solution", *The Canadian journal of chemical engineering,* vol. 67, no. 5, pp. 870-872.

Cournil, M. & Herri, J. 2003, "Asymptotic models for gas–liquid crystallization in two-film systems", *AIChE Journal,* vol. 49, no. 8, pp. 2030-2038.

Frank, M.J., Kuipers, J.A. & van Swaaij, W.P. 1996, "Diffusion coefficients and viscosities of CO2 H2O, CO2 CH3OH, NH3 H2O, and NH3 CH3OH liquid mixtures", *Journal of Chemical & Engineering Data,* vol. 41, no. 2, pp. 297-302.

Garcia-Ochoa, F. & Gomez, E. 2004, "Theoretical prediction of gas–liquid mass transfer coefficient, specific area and hold-up in sparged stirred tanks", *Chemical engineering science,* vol. 59, no. 12, pp. 2489-2501.

Han, B., Qu, H., Niemi, H., Sha, Z. & Louhi-Kultanen, M. 2014, "Mass Transfer and Kinetics Study of Heterogeneous Semi-Batch Precipitation of Magnesium

Carbonate", *Chemical Engineering & Technology,* vol. 37, no. 8, pp. 1363-1368.

Harned, H.S. & Davis Jr, R. 1943, "The ionization constant of carbonic acid in water and the solubility of carbon dioxide in water and aqueous salt solutions from 0 to 50", *Journal of the American Chemical Society,* vol. 65, no. 10, pp. 2030-2037.

Hostomsky, J. & Jones, A. 1995, "A penetration model of the gas-liquid reactive precipitation of calcium carbonate crystals", *Chemical engineering research & design,* vol. 73, no. A3, pp. 241-245.

Hövelmann, J., Putnis, C., Ruiz-Agudo, E. & Austrheim, H. 2012, "Direct nanoscale observations of CO2 sequestration during brucite [Mg (OH) 2] dissolution", *Environmental science & technology,* vol. 46, no. 9, pp. 5253-5260.

Hsu, J. & Liu, B. 1993, "Dissolution of solid particles in liquids: A reaction—diffusion model", *Colloids and surfaces,* vol. 69, no. 4, pp. 229-238.

Hsu, W., Lin, M. & Hsu, J. 2009, "Dissolution of solid particles in liquids: a shrinking core model", .

Hu, Z. & Deng, Y. 2004, "Synthesis of needle-like aragonite from calcium chloride and sparingly soluble magnesium carbonate", *Powder Technology,* vol. 140, no. 1, pp. 10-16.

Jones, A., Hostomsky, J. & Zhou, L. 1992, "On the effect of liquid mixing rate on primary crystal size during the gas-liquid precipitation of calcium carbonate", *Chemical engineering science,* vol. 47, no. 13, pp. 3817-3824.

Jones, A.G. 2002, *Crystallization process systems,* Butterworth-Heinemann.

Kakaraniya, S.J. & Mehra, A. 2007, "Reactive precipitation in gas-liquid systems", *Industrial & Engineering Chemistry Research,* vol. 46, no. 4, pp. 1125-1137.

Kotaki, Y. & Tsuge, H. 1990, "Reactive crystallization of calcium carbonate by gas-liquid and liquid-liquid reactions", *The Canadian Journal of Chemical Engineering,* vol. 68, no. 3, pp. 435-442.

Kudrewizki, F. & Rabe, P. 1986, "Model of the dissipation of mechanical energy in gassed stirred tanks", *Chemical engineering science,* vol. 41, no. 9, pp. 2247-2252.

Levenspiel, O. 1999, "Chemical reaction engineering", *Industrial & Engineering Chemistry Research,* vol. 38, no. 11, pp. 4140-4143.

Levich, V.G. & Technica, S. 1962, *Physicochemical hydrodynamics,* Prentice-hall Englewood Cliffs, NJ.

Lin, R., Zhang, J. & Bai, Y. 2006, "Mass transfer of reactive crystallization in synthesizing calcite nanocrystal", *Chemical engineering science,* vol. 61, no. 21, pp. 7019-7028.

Mersmann, A. 2001, *Crystallization technology handbook,* CRC Press.

Michel, B.J. & Miller, S. 1962, "Power requirements of gas-liquid agitated systems", *AIChE Journal,* vol. 8, no. 2, pp. 262-266.

Mullin, J.W. 2001, *Crystallization,* Butterworth-Heinemann.

Myerson, A. 2002, *Handbook of industrial crystallization,* Butterworth-Heinemann.

Nernst, W. 1904, "Theorie der Reaktionsgeschwindigkeit in heterogenen Systemen", *Z.phys.Chem.,* vol. 47, pp. 52-55.

Noyes, A.A. & Whitney, W.R. 1897, "The rate of solution of solid substances in their own solutions.", *Journal of the American Chemical Society,* vol. 19, no. 12, pp. 930-934.

Plummer, L.N. & Busenberg, E. 1982, "The solubilities of calcite, aragonite and vaterite in CO 2-H 2 O solutions between 0 and 90 C, and an evaluation of the aqueous model for the system CaCO 3-CO 2-H 2 O", *Geochimica et Cosmochimica Acta,* vol. 46, no. 6, pp. 1011-1040.

Pokrovsky, O.S. & Schott, J. 2004, "Experimental study of brucite dissolution and precipitation in aqueous solutions: surface speciation and chemical affinity control", *Geochimica et Cosmochimica Acta,* vol. 68, no. 1, pp. 31-45.

Rigopoulos, S. & Jones, A. 2003, "Modeling of semibatch agglomerative gas-liquid precipitation of CaCO3 in a bubble column reactor", *Industrial & Engineering Chemistry Research,* vol. 42, no. 25, pp. 6567-6575.

Rigopoulos, S. & Jones, A.G. 2001, "Dynamic modelling of a bubble column for particle formation via a gas–liquid reaction", *Chemical Engineering Science,* vol. 56, no. 21, pp. 6177-6184.

Sherwood, T.K., Pigford, R.L. & Wilke, C.R. 1975, *Mass transfer,* McGraw-Hill.

Tsutsumi, A., Nieh, J.Y. & Fan, L.S. 1991, "Role of the bubble wake in fine particle production of calcium carbonate in bubble column systems", *Industrial & Engineering Chemistry Research,* vol. 30, no. 10, pp. 2328-2333.

Vermilyea, D.A. 1969, "The dissolution of MgO and Mg (OH) 2 in aqueous solutions", *Journal of the Electrochemical Society,* vol. 116, no. 9, pp. 1179-1183.

Wachi, S. & Jones, A. 1991b, "Effect of gas—liquid mass transfer on crystal size distribution during the batch precipitation of calcium carbonate", *Chemical Engineering Science,* vol. 46, no. 12, pp. 3289-3293.

Wachi, S. & Jones, A.G. 1995, "Aspects of gas-liquid reaction systems with precipitate particle formation", *Reviews in Chemical Engineering,* vol. 11, no. 1, pp. 1-52.

Wachi, S. & Jones, A.G. 1992, "Dynamic modelling of particle size distribution and degree of agglomeration during precipitation", *Chemical engineering science,* vol. 47, no. 12, pp. 3145-3148.

Wachi, S. & Jones, A.G. 1991a, "Mass transfer with chemical reaction and precipitation", *Chemical Engineering Science,* vol. 46, no. 4, pp. 1027-1033.

Yagi, H., Iwazawa, A., Sonobe, R., Matsubara, T. & Hikita, H. 1984, "Crystallization of calcium carbonate accompanying chemical absorption", *Industrial & engineering chemistry fundamentals,* vol. 23, no. 2, pp. 153-158.

Yagi, H., Nagashima, S. & Hikita, H. 1988, "Semibatch precipitation accompanying gas-liquid reaction", *Chemical Engineering Communications,* vol. 65, no. 1, pp. 109-119.

Yuan-Hui, L. & Gregory, S. 1974, "Diffusion of ions in sea water and in deep-sea sediments", *Geochimica et Cosmochimica Acta,* vol. 38, no. 5, pp. 703-714.

Zemaitis Jr, J.F., Clark, D.M., Rafal, M. & Scrivner, N.C. 2010, *Handbook of aqueous electrolyte thermodynamics: Theory & application,* John Wiley & Sons.

LIST OF FIGURES